Antti Miettinen

Effects of Bias Voltages on Silicon Drift Detector Performance

Metropolia University of Applied Sciences

Bachelor of Laboratory Services

Laboratory Sciences

Bachelor's Thesis

1 October 2022

Abstract

Author:	Antti Miettinen
Title:	Effects of Bias Voltages on Silicon Drift Detector Performance
Number of Pages:	31 pages + 1 appendix
Date:	1 October 2022
Degree:	Bachelor of Laboratory Services
Degree Programme:	Laboratory Sciences
Professional Major:	
Supervisors:	Miika Kuivikko, Senior Lecturer

The thesis study was carried out for Hitachi High-tech Analytical Science Finland and the experiments were done in the clean room facilities in the company's Espoo offices. The thesis study is a part of a larger project to improve the production yield of an X-ray fluorescence silicon drift detector. The thesis focuses on the possibility that adjusting the bias voltages of the semiconductor chip can affect the analytical performance of the detector and finding the optimal voltages to maximize performance.

Three performance indicators were chosen for the study: FWHM (full width at half maximum), rise time and low energy tailing. FWHM of the Manganese Kα peak is a widely used indicator for the energy resolution of the detector and it measures the analytical accuracy of the detector. Rise time is a term used in electronics used to define the time it takes for a signal to be measured and is used in the thesis to measure the time it takes for the detector to measure an x-ray quantum. Low energy tail of the Mn Kα peak is an indicator of incomplete operation in the detector and for the thesis it is defined by dividing the integral of an area before the Kα peak by the peak height.

The measurements were made with 15 detectors that were outside the accepted parameters for at least one of the indicators and 1 that was within the limits. Around 60 sets of voltages were measured for each detector.

The results of the experiments were that adjusting the bias voltages influenced FWHM and rise time but did not affect the low energy tail. The optimal bias voltages for minimizing FWHM and rise time according to the experiments were R1 = 120V-140V, R18= 270V-340V, BC = 240V-220V.

Keywords:	XRF, SDD, bias voltage

Tiivistelmä

Tekijä:	Antti Miettinen
Otsikko:	Bias-jännitteiden vaikutus pii-drift-detektorin toimintaan
Sivumäärä:	31 sivua + 1 liite
Aika:	1.10.2022
Tutkinto:	Laboratorioanalyytikko (AMK)
Tutkinto-ohjelma:	Laboratorioanalytiikka (AMK)
Ohjaajat:	Lehtori Miika Kuivikko

Opinnäytetyö tehtiin yritykseen Hitachi High-tech Analytical Science Finland ja mittaukset toteutettiin yrityksen puhdastiloissa Espoossa. Työ on osa suurempaa projektia parantaa erään röntgenfluoresenssin pii-drift-detektorin tuotannon saantoa. Tarkemmin työ keskittyi bias-jännitteiden muuttamisen vaikutukseen detektorin toimintaan ja tavoite oli löytää optimaaliset jännitteet suorituskyvyn maksimoimiseksi.

Työhön valittiin mitattavaksi kolme toimintakyvyn indikaattoria: puoliarvoleveys, nousuaika ja matalaenergiahäntä. Mangaanin Kα-piikin puoliarvoleveys (FWHM) on yleisessä käytössä oleva indikaattori detektorin energiaresoluutiolle, ja se kuvaa detektorin analyyttistä tarkkuutta. Nousuaika on elektroniikassa käytetty termi, joka kuvaa signaalin mittausnopeutta. Tässä työssä se kuvaa, kuinka nopeasti röntgenkvantin energia mitataan. Mangaanin Kα piikin matalaenergiahäntä kuvaa varauksenkeräyksen täydellisyyttä signaalissa. Matalaenergiahäntä määrittää Kα-piikin edessä olevan alueen integraalin suhdetta piikin korkeuteen.

Mittaukset tehtiin 16 detektorille. 15 detektoria oli vähintään yhdellä mittausparametrillä ohi tuotannossa asetetuista rajoista. Jokaiselle detektorille tehtiin mittaukset noin 60 bias-jännitteellä.

Mittausten tulokseksi saatiin, että puoliarvoleveyteen ja nousuaikaan pystyttiin vaikuttamaan jännitteiden säädöllä, mutta matalaenergianhännässä ei havaittu muutosta. Työn johtopäätös on että, puoliarvoleveyden ja nousuajan minimoimiseksi bias jännitteet tulisi säätää alueille R1 = 120V–40V, R18= 270V–340V, BC = 240V–220V.

Avainsanat:	XRF, SDD, bias-jännite

Contents

List of Abbreviations

ASIC: Application specific integrated circuit. A chip customized for a particular use, rather than general purpose only

BC: Back contact. The term for the bias voltage directed to the side opposite the anode or the entrance window side in a silicon drift detector.

FWHM: Full width at half maximum. The distance between points on a curve at which the function of the curve reaches half of its maximum value.

SDD: Silicon drift detector. Radiation detector used in x-ray spectrometry

XRF: X-ray fluorescence. A way of measuring elements using x-ray

1   Introduction

The thesis study was carried out for the XRF (X-ray fluorescence) detector development team of Hitachi High-tech Analytical Science Finland. The company designs and manufactures elemental analysers and components for the company, and the detector development team oversees designing the detectors and supporting their manufacturing.

The study is a part of an ongoing project to improve the production yield of a certain type of detector. Earlier internal measurements raised the possibility that adjusting the biasing voltages of the detector could improve performance without the need for more extensive and expensive repairs and the study is a series of more in-depth measurements for a larger range of possible bias voltages. If the measurements show that adjusting the bias voltages can improve the yield the plan is to explore the possibility of an automated system for the adjustments, instead of the fairly time and resource intensive manual system used in the study. The system is in active use by the manufacturing team and measurements were done when it was not in use for normal manufacturing needs.

The project to improve the yield is a co-operative one with another company under the Hitachi umbrella in Japan, supplying Hitachi High-tech Analytical Science Finland with the semiconductor crystals used in the detectors.

2   X-Ray Fluorescence

X-rays are radiation with a shorter wavelength, and therefore of higher energy than visible light. X-rays can be used to release electrons from their energy shells around the nucleus of an atom. The innermost electron shell around the nucleus is called K and it has two electrons. When an electron from the K-shell is released by absorbing the required energy, from X-rays in this case, an electron from a higher shell transition to the vacancy on the K-shell. If the electron comes from the next shell L, the resulting emission is called K_α, and if it is from M-shell, it is called K_β. The transitions are visualized in figure 1. [1, p.1-3.]
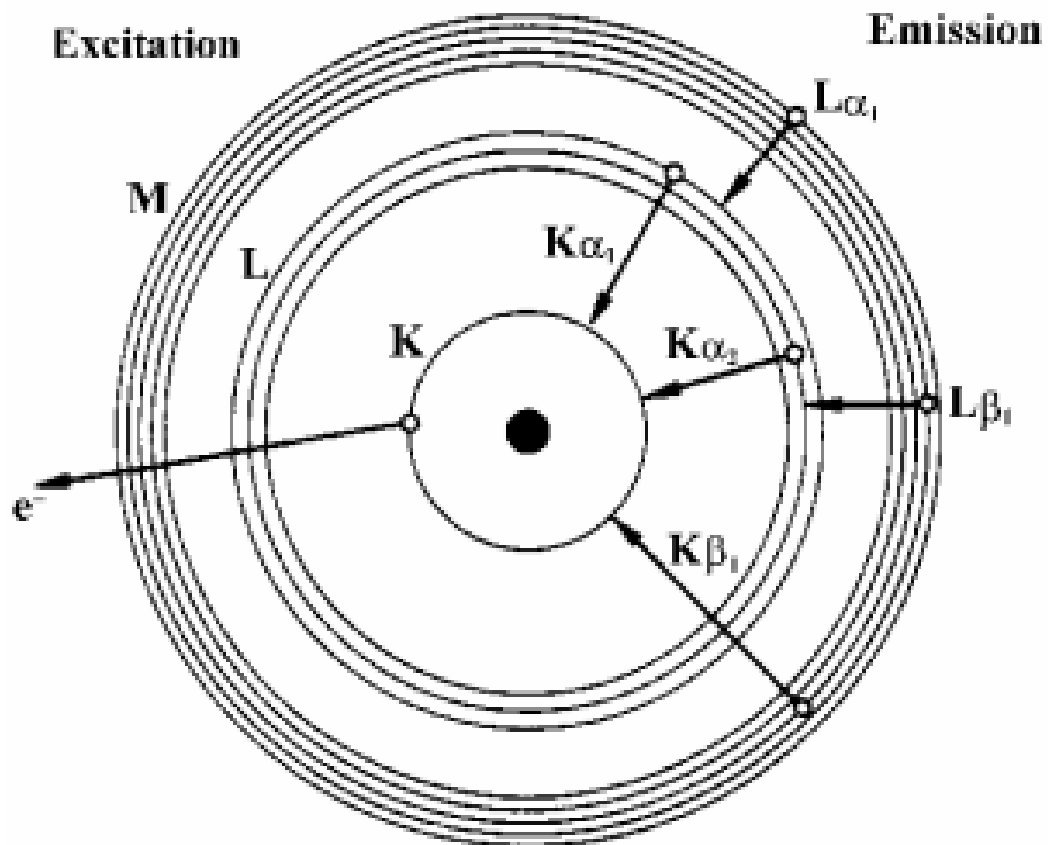
Figure 1. Electron transition in the Bohr atomic model [1, p.2].

The basis of XRF is that the emission caused by electron transfer is characteristic for each element, and due to the fact the energies of the electrons

on the shells are constant so the transition is always the same [2]. In this project the atom is energized by a controlled X-ray source and the emission is measured by an energy dispersive detector. Using these methods all elements between Beryllium and Uranium can be detected in principle, although results depend on the used instrument [3, p.1].

The detector converts all the incoming photons to an electrical signal and as these signals are processed by a multichannel analyser, a continuous spectrum is generated [2]. When a sample is energized by x-rays, some of the energy is scattered by natural processes, causing radiation background [1 p.11]. The goal of the measurement instrument is the to minimize the background signal and full width at half maximum (FWHM) of the elemental peaks. [2.]

An example of an XRF spectrum can be seen in figure 2. It is the spectrum of a radioactive Fe-55 source, where the highest peak is the Kα peak of manganese at 5895 eV, and the next peak is the Kβ peak [2]. The higher energy peaks later in the spectrum are pileup K peaks [2] and the peaks before are escape peaks caused by the silicon in the detector [1, p. 21]. Fe-55 shows the XRF-spectrum of manganese because it is a radioactive substance that decays into manganese [4].
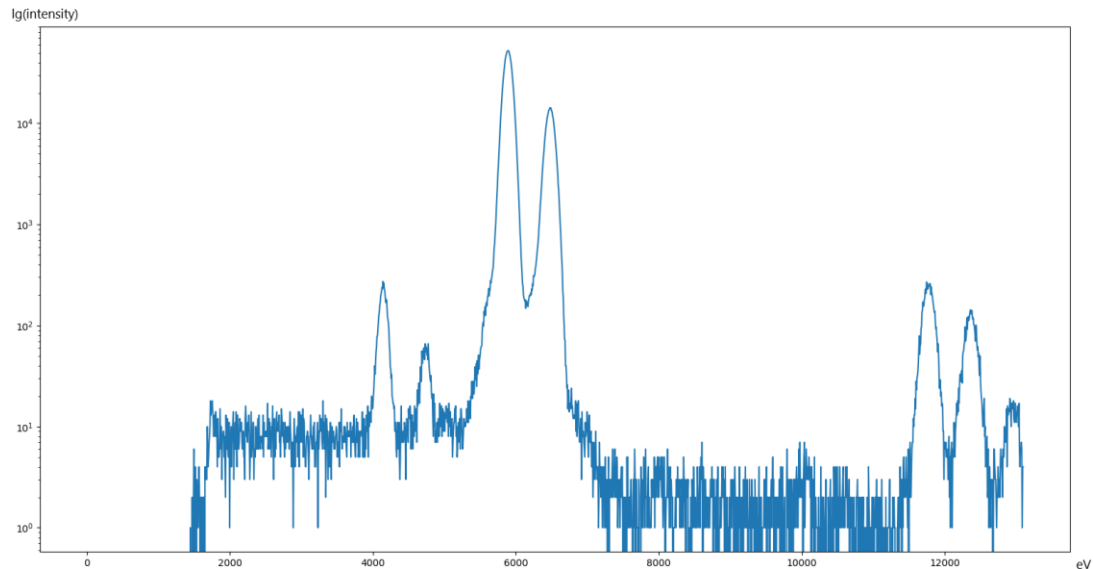
Figure 2. Fe-55 spectrum logarithmic intensity as a function on eV.

The detector is the heart of an XRF instrument and defines its measurement fidelity. There are several ways to improve the functionality of a detector. The detector needs to be cooled to an operation temperature to minimize leakage current. The operational temperature depends on the device and the quality of the crystal, with the temperature set from near 0 °C to much lower. Then to prevent ice from forming on the surfaces of the detector a vacuum is needed. The vacuum sealed capsule has a beryllium window that allows the x-rays to pass through but maintains the vacuum. The signal is then turned into a readable spectrum by the detector components and a pulse processor. The detector and pulse processor together form an XRF spectrometer. A picture of a detector and pulse processer can be seen in figure 3. [2.]
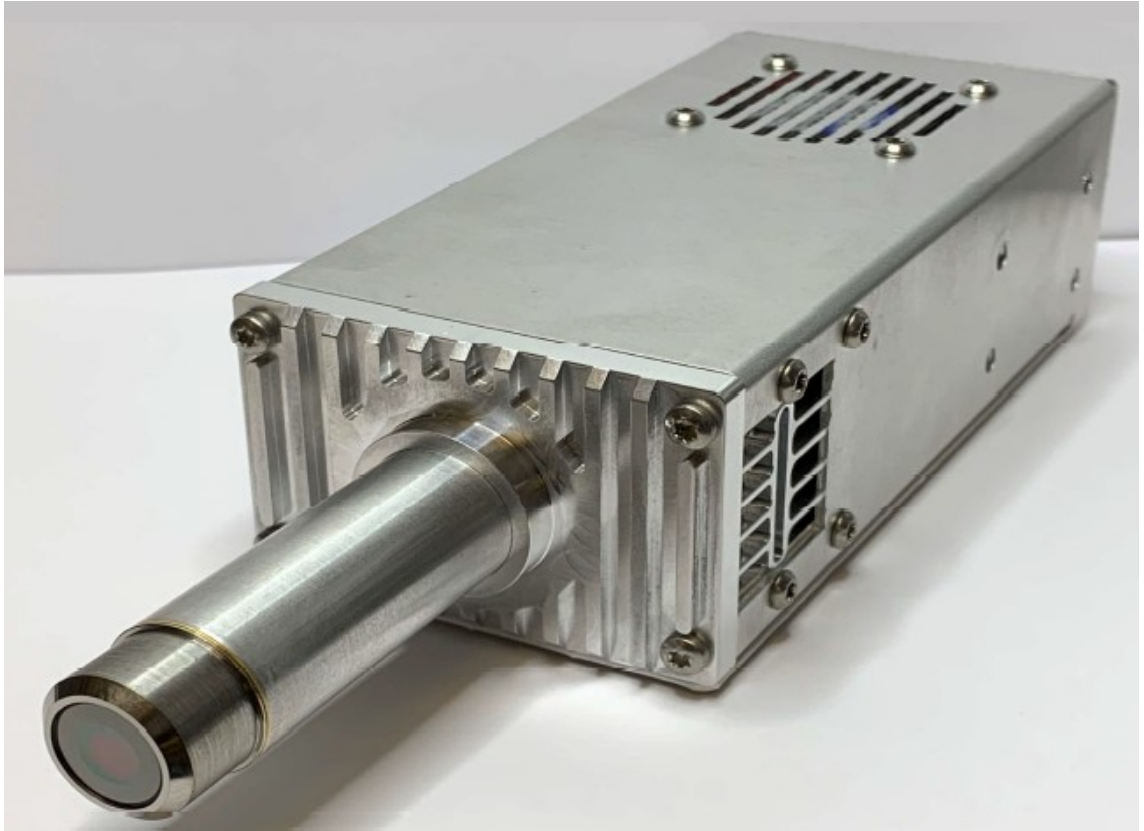
Figure 3. An XRF spectrometer

3 Silicon Drift Detector

3.1 Components

Inside the detector behind the beryllium window is a collimator which confines the incoming radiation so that it only enters the silicon crystal. The collimator can be made from many materials depending on the product. [2.] Behind the collimator is the detector crystal, which is explained more thoroughly later.

The crystal is adhered to a substrate package that acts as a contact between the crystal and the rest of the components. The package is made with pure materials with good thermal conductivity. The substrate consists of an application specific integrated circuit (ASIC) which amplifies the charge signal from the crystal, a thermistor to monitor the temperature and wire bonds to make the electrical contacts. The wire bonds are 17.5 μm thick aluminium wire. [2.]

After the substrate is the peltier element, which transfers and creates heat. The peltier is used for temperature regulation because it can be optimized for different energy consumptions for different devices and reliability because a peltier has no moving parts [5].

The peltier is bonded to the header, which is the connection point between the inside and outside of the detector capsule. The header is gold plated to improve weldability and contains a copper tube to allow the pumping of the vacuum. The most important quality for the header is leak tightness to maintain the vacuum. [2.]

A getter is adhered to the inside of the capsule and is made of a material that can absorb any degassing arising inside capsule after it is welded shut and the vacuum is pumped. [5.] The components can be seen labelled in figure 4.
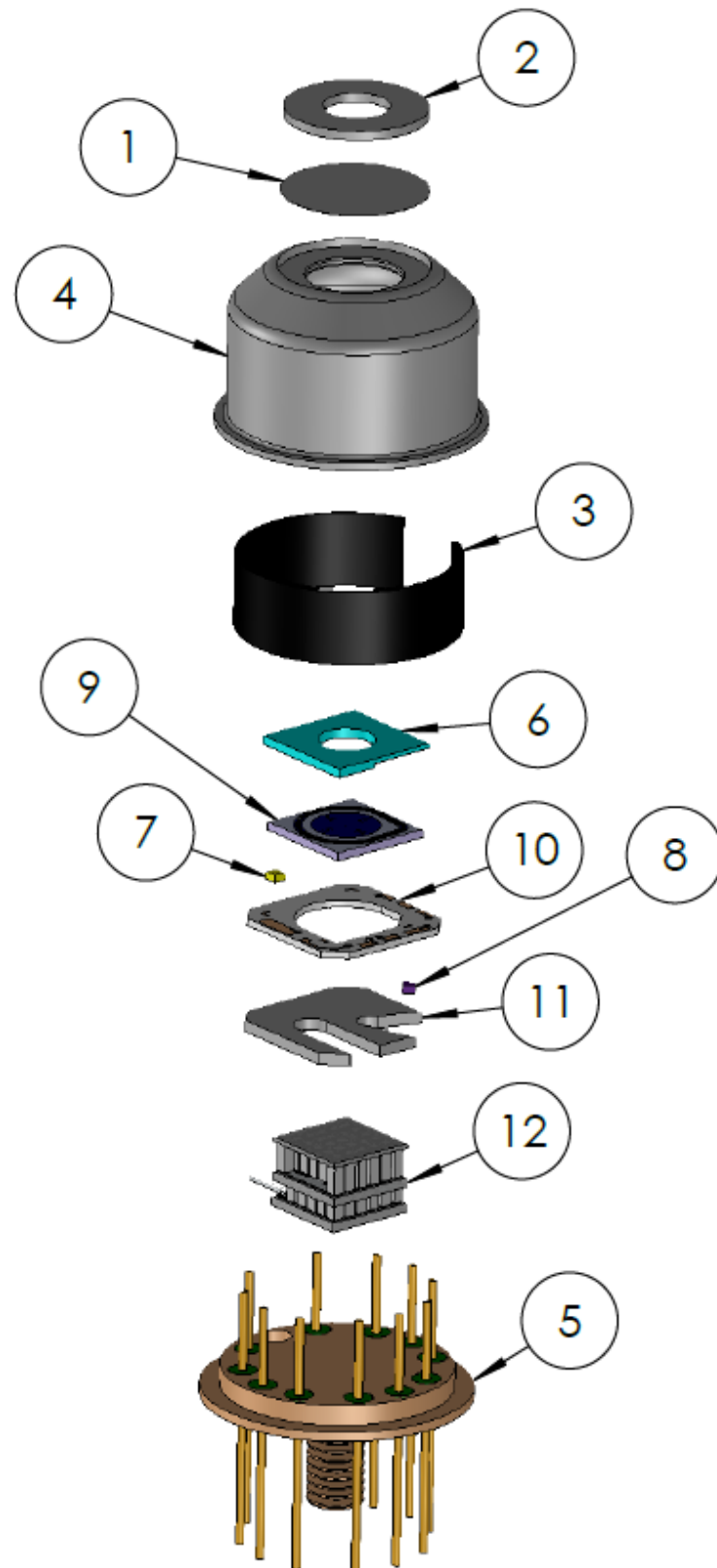
Figure 4. Detector components: 1. Beryllium window 2. Collimator 3. Getter 4. Capsule 5. Header 6. Collimator 7. Thermistor 8. ASIC 9. Silicon detector crystal 10 & 11. Substrate 12. Peltier [2].

3.2 Crystal

As the detector is the heart of the analytical instrument, so the semiconductor crystal is the heart of the detector. The crystal is made from silicon. Pure silicon is an insulator and called i-type, but by adding elements into silicon its properties can be changed. By adding phosphorous silicon becomes n-type and by adding boron it becomes p-type. These three types of silicon are then used to manufacture many electronical components. [2.]

In a SDD (Silicon Drift Detector) most of the crystal is high purity n-silicon, with a large cathode contact made of p-silicon. On the other side around an anode is a series of concentric rings made of p-silicon. The construction of a SDD is shown in figure 5. [6.] The plus-designation in the silicon types means that these thin layers have unusually high concentration of impurity which causes high conductivity. The layers are usually used in making electrical contacts in semiconductor components. [7, p.375.]
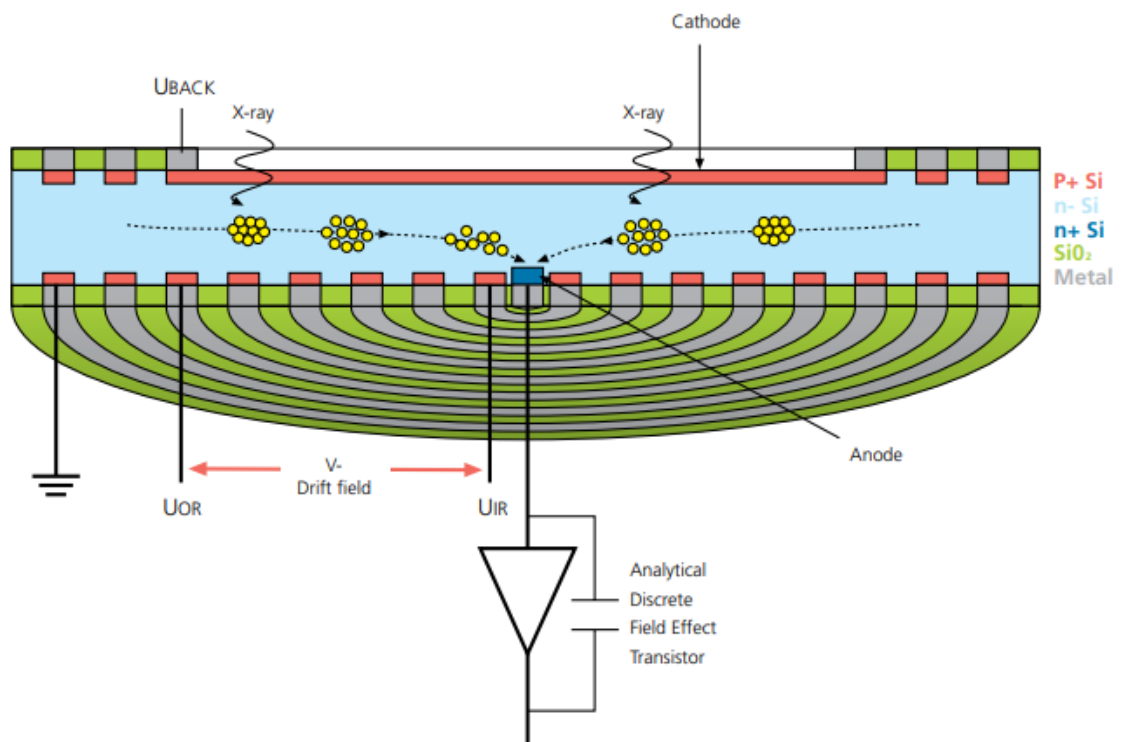
Figure 5. SDD crystal construction [6]

A detector constructed like this would work, but with poor performance, which is why a biasing voltage is used to improve performance [7, p.382]. The detector is reverse biased until the n-type silicon is fully depleted [7, p.506]. Reverse biasing means directing a negative voltage to the p-silicon regarding the n-type. This is done to allow the charges generated by the XRF to be measured [8]. Silicon depletion is a term in semiconductor physics meaning an area of a semiconductor where the flow of charge carriers is decreased until the area is empty of mobile charge carriers or full of immobile carriers [9].

When an XRF quantum travels into the detector silicon, it begins to interact with the silicon atoms inside. Every time the quantum collides with an atom, it loses 3,6 eV energy and continues to lose energy every collision until it is attenuated or leaves the crystal. The energy of the quantum causes electron hole pairs for each atom it collides with. This charge cloud, or pulse, is directed by the biasing to the anode where the charge is measured. [8.]

A p-n junction in silicon will conduct current when the p-side is made positive with respect to the n-side. This is called forward biasing and when reversed the junction allows the electrons to flow from the p-side and the holes from the n-side. When a junction is reverse biased all the voltage will affect the whole depletion range, because the resistivity of the junction is much higher than a forward biased one. This also causes the volume of the depletion area to grow. [7, p.382-383]

In a silicon crystal the electrons have energies inside defined energy bands. These energy bands are separated by gaps of forbidden energies. Two bands are of interest in the case of a drift detector. The lower band is called the valence band and the next higher is called conduction band. Valence electrons are part of the interatomic crystalline structure of the silicon. Conduction electrons are free to move through the crystal and contribute to the electrical conductivity of a material. The gap between these bands determines whether a material is a semiconductor or an insulator. The number of electrons in a material is exactly enough to fill the valence band and without thermal excitation

there would be no difference in the electrical conductivity of a semiconductor and an insulator. The bands are shown in figure 6. [7, p.366]
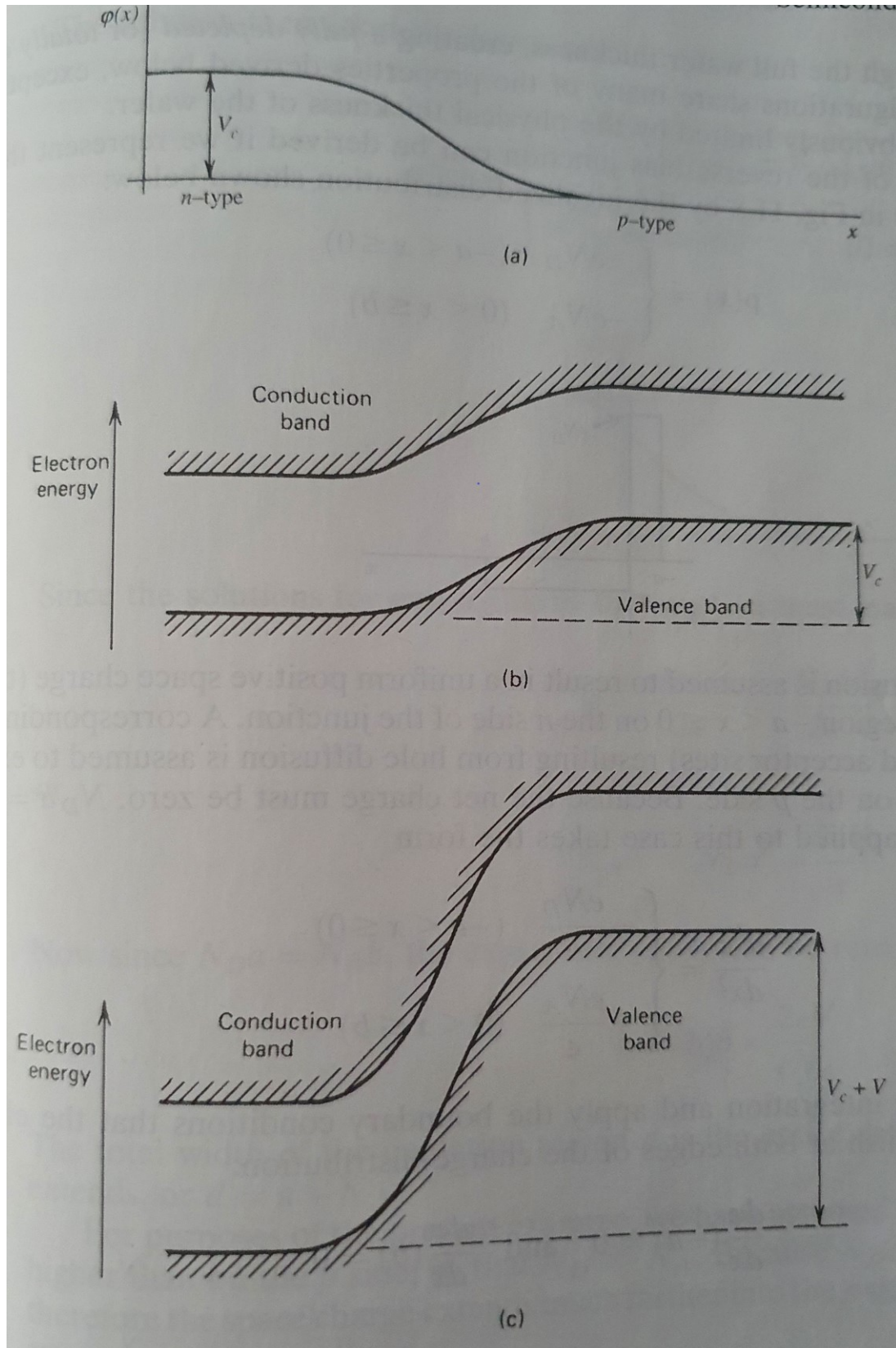
Figure 6. (a) Variation of electric potential at the p-n junction. (b) The difference in electron energy bands. (c) Increased difference in the bands caused by reverse biasing [7, p. 383].

A fully depleted crystal has no electrons in the conduction band, but when excited, an electron moves to the conduction band and creates a vacancy in the valence band. This combination is called an electron-hole pair and the electrical field applied to the crystal will affect the migration of the pair. The hole, with a net positive charge when compared to the electron, will tend to move in an opposite direction to the electron. The motion of these charges contributes to the measured electrical conductivity of the crystal. [7, p.367.]

The motion of the electron-hole pair is a combination of random thermal diffusion and a drift velocity that is parallel to the applied electrical field. The drift velocity is dependent on the strength of the electrical field. At low values the velocity is proportional to the field, but in a silicon drift detector the electrical field is strong enough to reach saturation velocity where increase in the strength of field no longer increases velocity. At the saturation velocity the time it takes for the charge reach the anode is roughly 10 ns. [7, p.368-369.]

The anode is made as small as possible to minimize capacitance. Because of the design of the concentric rings electrons can drift from a larger area than in other semiconductor detectors with smaller capacitance. Detector capacitance is a major factor in spectrometer noise and lower is better. Leakage current caused by temperature is a major factor in FWHM, but a silicon drift detector does not need operational temperatures as low a lithium drifted detector, which is cooled with liquid nitrogen and used to be the industry standard [7, p.506-507].

Charge measurement happens in the electronical components connected to the crystal and is not instant. While a charge is measured if the charge of another quantum reaches the anode it is not measured. After the charge hits the anode the pre-amplifier in the detector gathers the charge for a set amount of time before the charge is released the energy is measured, creating a ramp. The time set is called peaking time and it is around 1 µs. A shorter peaking time means fewer quanta are missed, but also lowers the fidelity of the measured peaks. [10.]

The percentage of ignored charge is called deadtime. Deadtime depends on the input count rate, peaking time, and the temperature of the detector. The relationship between input rate and output rate is linear in the operational input range of any given detector. Temperature affects the length of the linear area. The linear area of deadtime is shown in figure 7. The optimal dead time is at the higher end of the linear area, because when the input rate is higher the sample spectrum gathers faster allowing faster and more accurate measurement, without the loss of efficiency caused by the nonlinear dead time at a too high input rate. [10.]
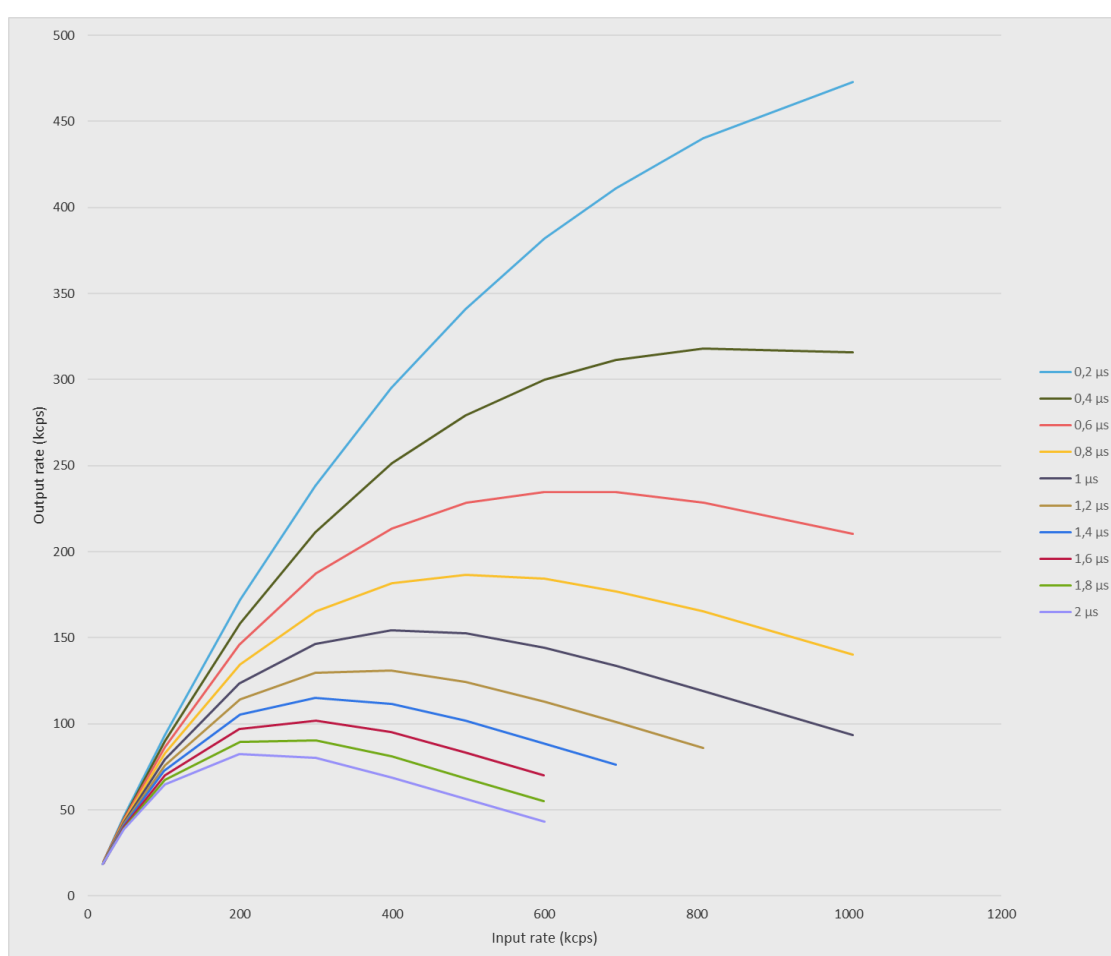
Figure 7. The linear and non-linear area of deadtime by input count rate at different peaking times.

The size of the crystal determines how well the energy of the XRF quanta is captured. A thicker crystal causes the quantum to collide with more atoms

before leaving and a larger diameter allows for more quanta to be measured. However, a larger crystal also requires a stronger electrical field to maintain depletion. [8.] Industry standard for the active surface area of a SDD is roughly 10-100 mm^2 and the crystal thickness is 0.5 mm [2].

3.3   Bias and Noise

The electron released by the XRF quantum are caught by the electrical field caused by the biasing. Biasing is designed so that there is a constant flow from the outside edge of the cathode to the anode. The result of this is that mostly only the electrons are measured at the anode. Some charge not caused by the XRF quantum is inevitably also measured. This causes noise and the low operational temperature is one of the ways to minimize it. [8.]

Due to the needed strength of the electrical field, at least a hundred volts, needed to fully deplete the crystal, at least some conductivity is shown. This causes a steady leakage current. Fluctuations in the leakage can mask smaller signal currents causing noise. The drift ring configuration is a design choice made to minimize leakage. [7, p.379.]

Leakage current is the most significant cause of noise in a silicon detector followed by surface leakage and other causes. The relative impact of these sources depends on the magnitude of the leakage, the capacitance of the crystal anode and if the crystal is completely depleted. [7, p.394.]

Surface leakage occurs at the edges of the p-n-junction because a relatively large energy gradient is supported over a small area when the bias voltage is applied to the crystal. The amount varies greatly depending on many factors. Clean encapsulation techniques are a major factor, and the detectors used in this project are manufactured inside a clean room. Other causes can include fingerprints on the detector surface, other oils, or condensable vapours. [7, p.393.]

Other causes of noise include electrons ending up in the inner most ring of p-silicon, called R1, which can occur if the biasing voltages are not optimally set. Diffusion also increases in higher temperature, which is one of the reasons for the low operational temperature. The electrical field is weaker nearer the edge of the crystal causing electrons to move slower or escape to the edge. [8.]

Low energy tailing can be caused by several causes. One of them is that if the electrical field is too weak, electrons can recombine or be trapped on the way to the anode. Radiation causes these types of traps inside the crystal and as the detector ages more traps form and fidelity decreases. Thermal diffusion also causes low energy tailing. [8.]

Risetime in a silicon detector is limited by the time it takes for the charge cloud generated to move from the edge of the crystal to the anode. These times are minimized with the high electric field and by the thickness of the crystal. Because the electrical field is not fully uniform inside the crystal there is variance in the risetime. [7, p.395.]

The high fidelity of a silicon drift detector is dependent on the near perfect crystalline lattice of the silicon atoms preventing trapping by defects. Extensive use of the detector causes more defects due to the disruptive effect of the x-ray quanta measured as they pass through the crystal. The creation of the electron-hole pairs is fully reversible, but nonionizing energy transfers to the atoms in the crystal causes irreversible changes. The most common type of damage is called Frenkel defect, where a silicon atom is displaced from its lattice position. The new vacancy and the atom now in an interstitial position causes a trapping point. These, and other types of defects, accumulate until the detector no longer functions, limiting the lifetime of a detector to a few years of active use. [7, p.398.]

4   Measurements

The measurements were done with a setup where the detector is in a vacuum chamber and the bias voltages were modified by turning dials on the chamber's side. A diagram of the test setup is in figure 8.
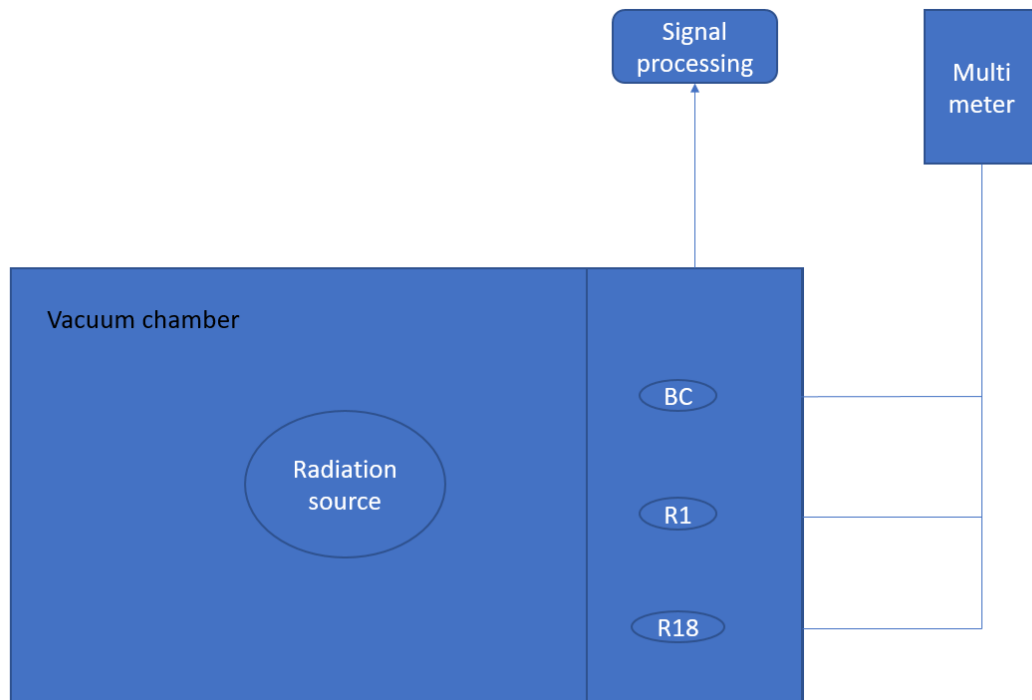
Figure 8. The measurement setup

The outgoing signal from the detector was then processed and the three desired values were recorded. The measured values were FWHM Mn tail and risetime. FWHM was measured using the Gaussian method [11].

Mn tail is a low energy tail on the Mn Kα-peak. It is an internal testing parameter for the quality of the detector. It is defined as the integral of the spectrum between 4381-5670 eV divided by peak height at 5895 eV. For the measured detector the limit is 0,8 %. [11.] Mn tail shows charge that is lost before the signal reaches the anode and it is caused by several different factors [8].The amount of charge lost depends on the distance the pulse traveled inside the

crystal before reaching the anode, therefore loss is variable, and it is spread only to the low energy side [7, p.394].

Risetime is the time it takes for a signal to cross the distance between a determined lower and higher value [12]. In this project it is defined by the time it takes for the energy of a single energy ramp to be registered by the pulse processing unit. Rise times were measured 1000 times for each set of bias voltages. The results were gathered in a histogram and the centroid and standard deviation of the histogram were recorded.

The measurements were done by adjusting three different bias voltages: R1, R18 and back contact (BC). R1 is the voltage directed at the closest p-type silicon drift ring to the anode and R18 to the X closest ring. The term R18 is generally written as RX but used in the measurements and figures as R18 due to legacy annotation in the company and is not the 18th closest ring in the measured detector. BC voltage is directed to the side opposite the anode, as shown in figure 9.
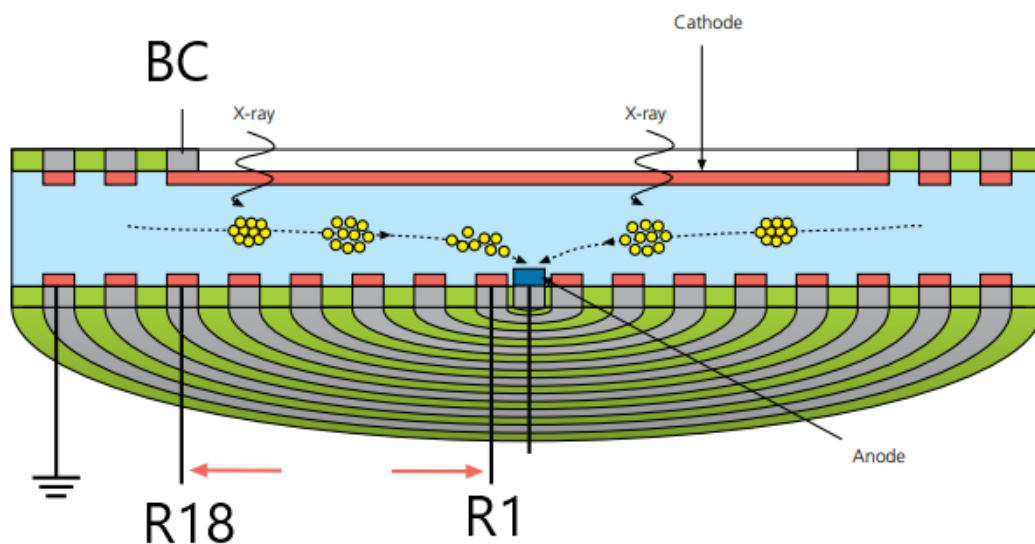
Figure 9. Bias voltage contacts [6]

The ranges for the three voltages were adjusted during the project. The first detector measured only had adjustments made to R18 and BC, but subsequent measurements were done with varying R1 voltages as well. The range for R1 was 140V-60V. The range for R18 and BC varied between detector and R1 voltages.

The measurements for a detector were started by first adjusting R1 to a voltage of 140V and then setting R18 to 310V and then finding the boundaries of BC. Beyond the upper BC boundary, the spectrum lost its shape as the low energy area before Mn Kα-peak began to rise, as shown in figure 10. At the lower boundary of BC, deadtime was no longer constant.
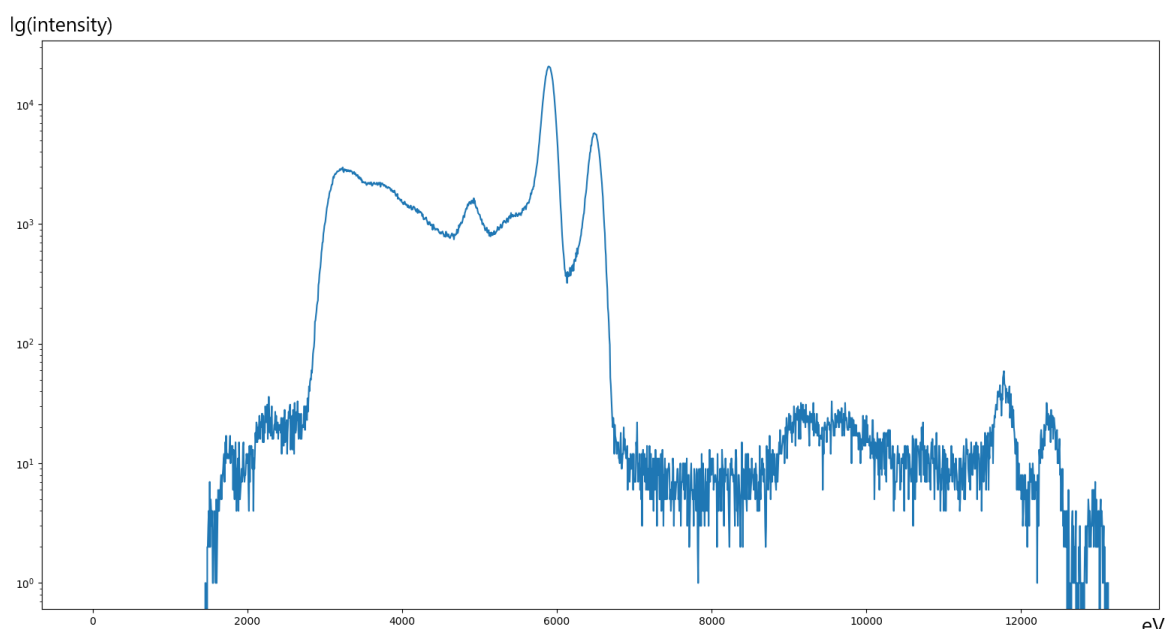
Figure 10. A spectrum with BC beyond the upper boundary

For the first three detectors measured the extremes of BC voltages measured were these boundaries, but from then on, a 10V buffer was in use at the boundaries. After the BC range was measured in 15-30V increments, R18 was lowered by 30 V and the BC range was reacquired. R18 had no impact on the upper BC boundary, but a lower R18 voltage raised the lower boundary of BC. When a R18 voltage with no suitable BC values was reached, R1 was lowered by 20V and R18 was set to 310V again. The maximum voltages for R1 and R18

were defined by the maximum the electrical components of the completed detector can handle. R1 determined the upper boundary of BC. There were some small differences between detectors, but when R1 was lowered, the upper boundary of BC lowered the same amount. The original BC boundary when R1 was 140V varied between detectors. An example of the measurement for the range of a single detector is in figure 11. For each set of voltages, a single 30 second measurement was made.
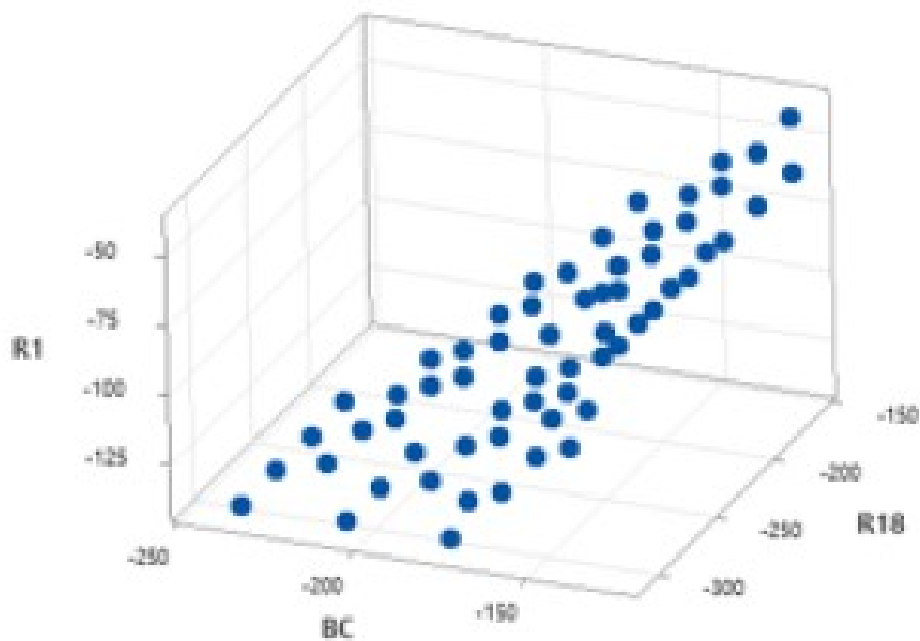
Figure 11. Measurements for a single detector

A total of 16 detectors were measured during the project. One that passed the internal production testing and 15 that failed.

5   Results

The results for each measured value are examined separately. All three values were measured for all bias voltage sets. Only three detectors are examined in detail to limit the number of similar figures in the report. The three detectors examined in this chapter are the one that passed internal production testing (06_PASS), a failed one where the SDD-crystal is from the same silicon wafer as the passed one (06_FAIL) and a second failed one from a different wafer (02_FAIL).

The spectra of all measurements for each of the three detectors are in figure12. The spectra all normalized so that the highest peak measured is at 5895 eV to allow direct comparison between measurements.
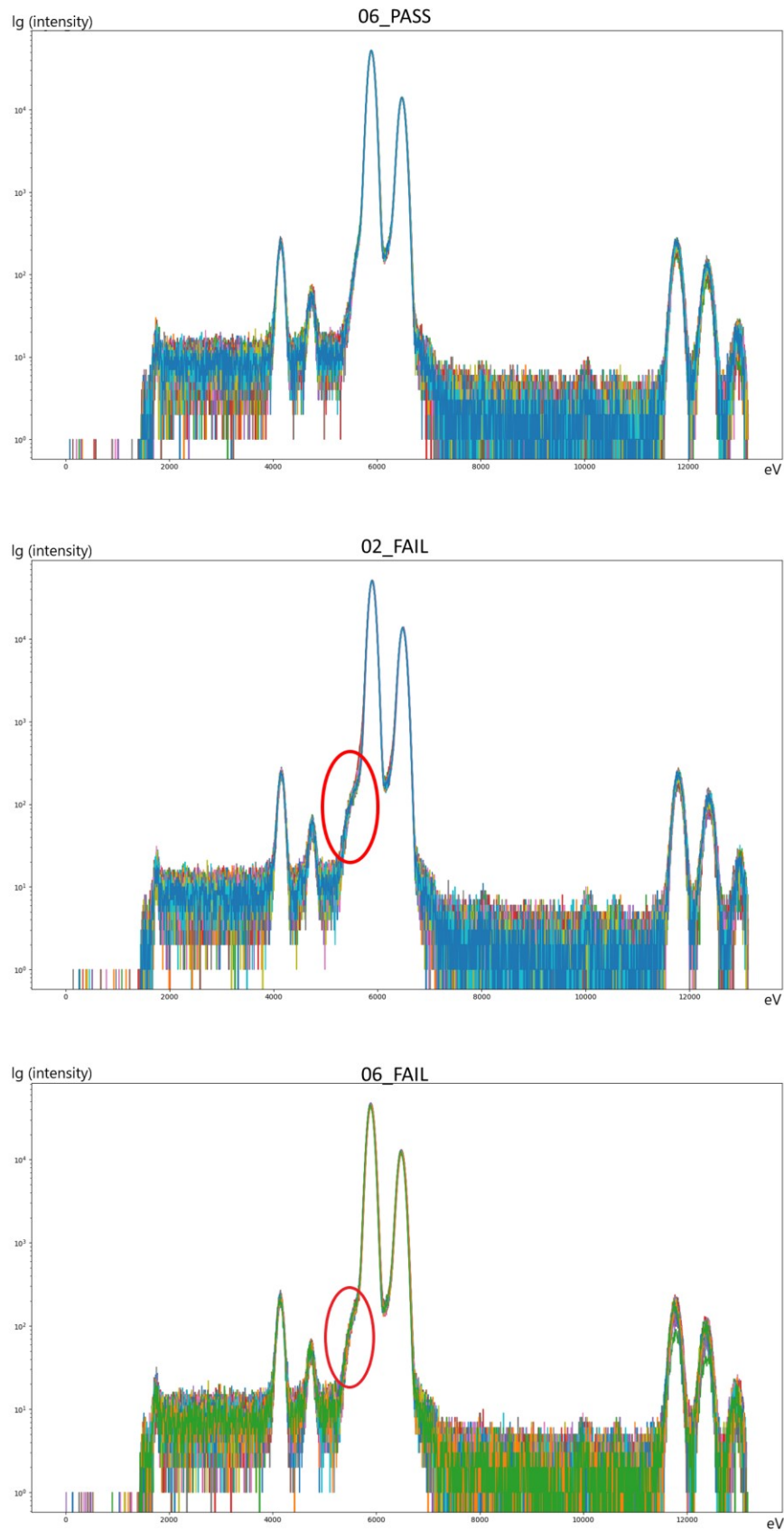
Figure 12. The spectra of the three detectors. Low energy Mn tail circled in red.

As the figures show, the spectrum changed very little between measurements. The difference between the failed and passed detectors can be seen as a low energy bump at around 5500 eV on 02_FAIL and 06_FAIL that is remarkably smaller on 06_PASS. Full results are shown in appendix 1.

5.1 Mn tail

Mn tail results for the three detectors are represented in figures 13, 14 and 15. The results were recorded with a single significant figure, because for the purposes of the normal manufacturing process the value is sufficiently clear.
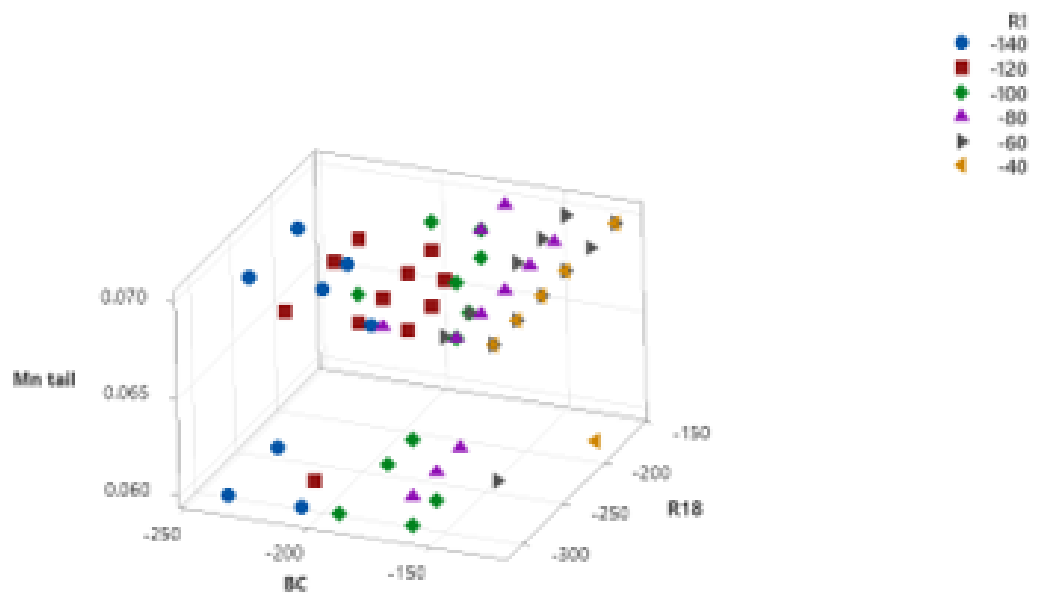
Figure 13. 06_PASS Mn tail measurements
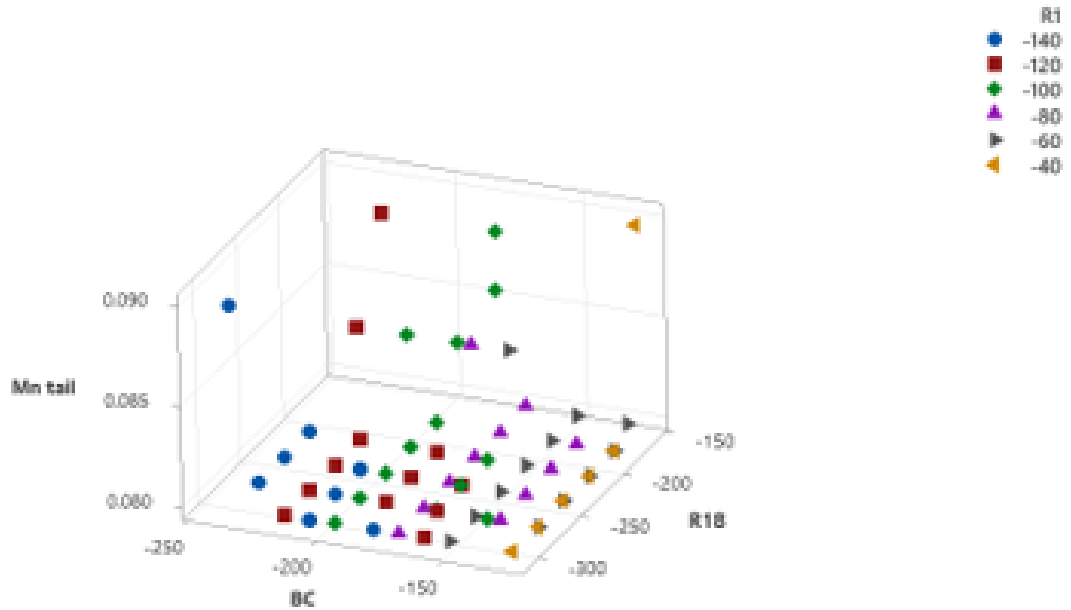
Figure 14. 06_fail Mn tail measurements
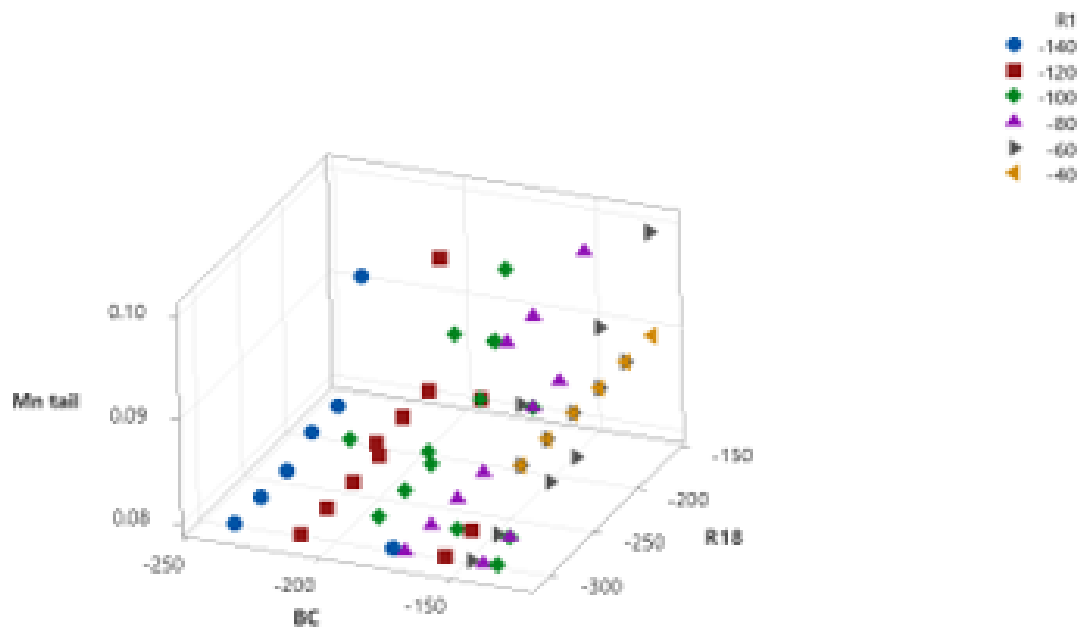
Figure 15. 02_FAIL Mn tail measurements

In the figures none of the voltages have a predictable or noticeable effect on the value of Mn tail. The value is mostly constant for all detectors with all bias voltages and only varies roughly 0.02% from a baseline typical to each detector. A few extreme measurements returned much worse results with higher Mn tail

values, but for those measurements either FWHM, risetime or both were also outside of expected ranges.

5.2   FWHM

FWHM results are in a series of six in figures 16, 17 and 18. The results are separated by R1, with the contour scale being the same for each of the first five figures. The last one is a scatterplot, because as figure 9 showed the viable BC range shrinks as R1 approaches 0, so R1 and BC are both constant. The scatterplot has reference lines showing the contour levels.
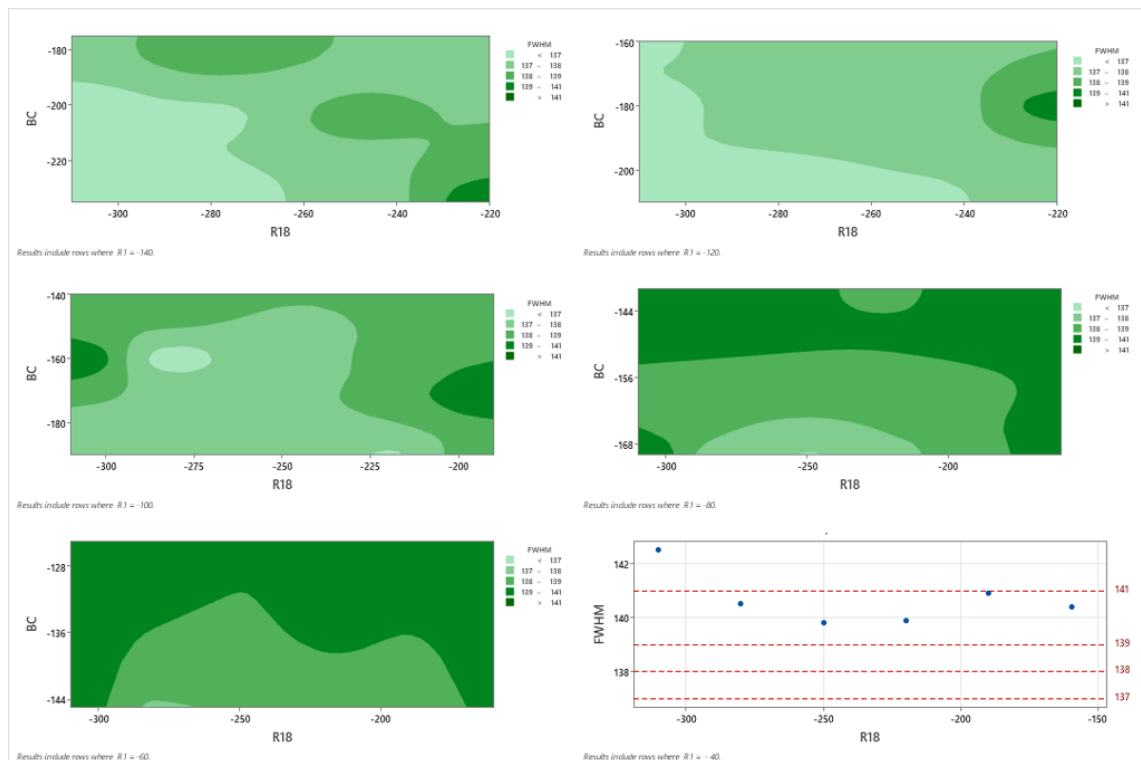
Figure 16. 06_PASS FWHM results separated by R1 value.
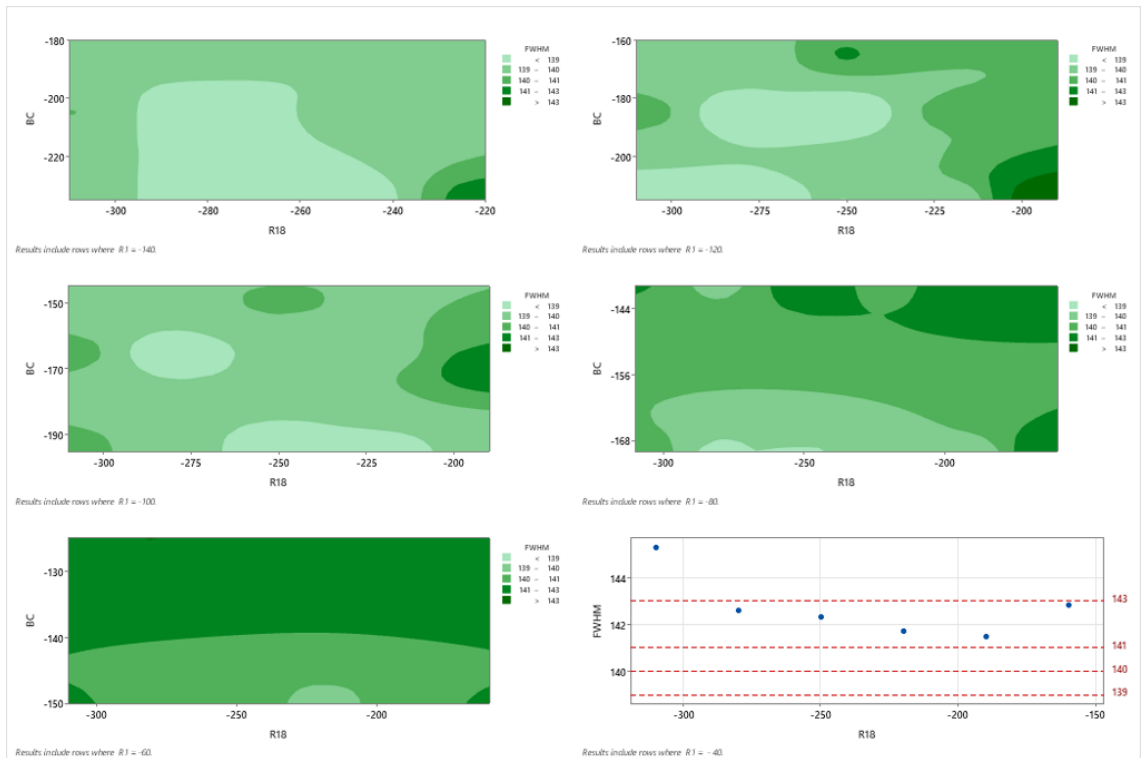
Figure 17. 06_FAIL FWHM results separated by R1 value.
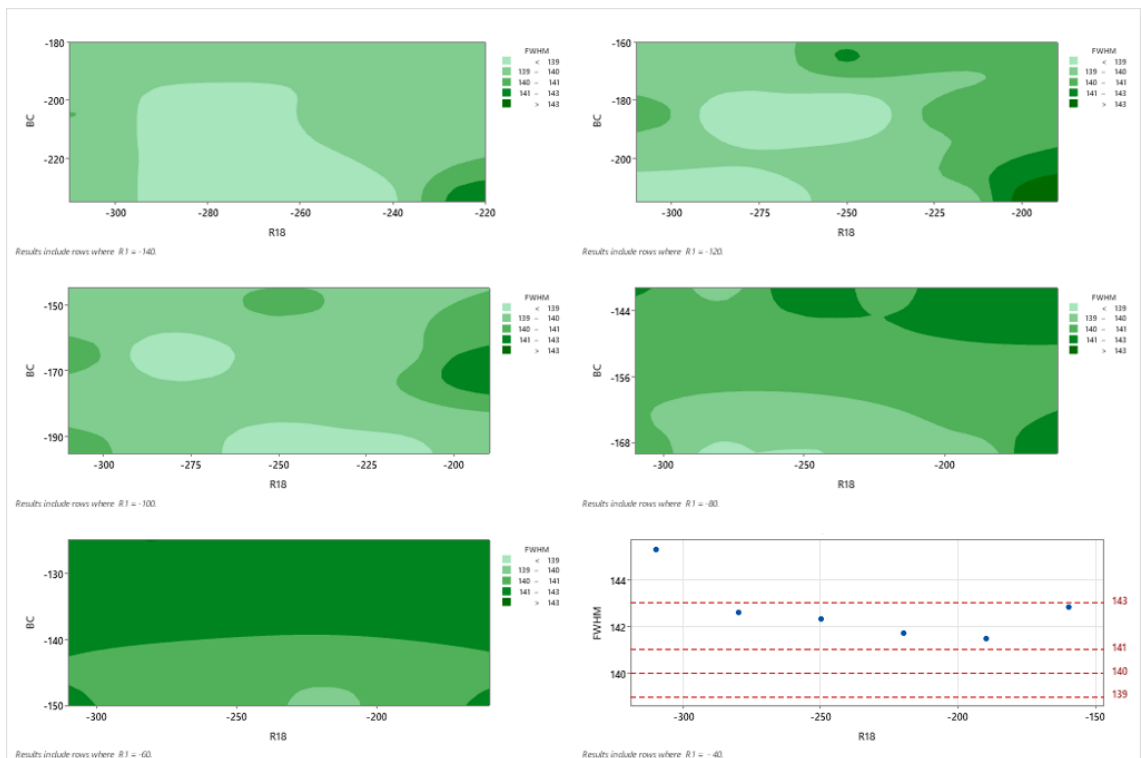
Figure 18. 02_FAIL FWHM results separated by R1 value.

The figures show that as R1 approaches 0, FWHM increases. In the R1 = -140V figures the highest levels of the contour are not present, but in R1 = -40V only the two highest contours can be seen. The FWHM values vary between detectors, but the behaviour is similar.

The effects of R18 are less pronounced, but the lowest values of FWHM are in the centre of the X-axis and increase when either boundary is approached.

For BC the lowest values of FWHM correspond with the highest BC values, which are lower on the Y-axis.

5.3 Risetime

Risetime results for the three detectors are in figures 19, 20 and 21.
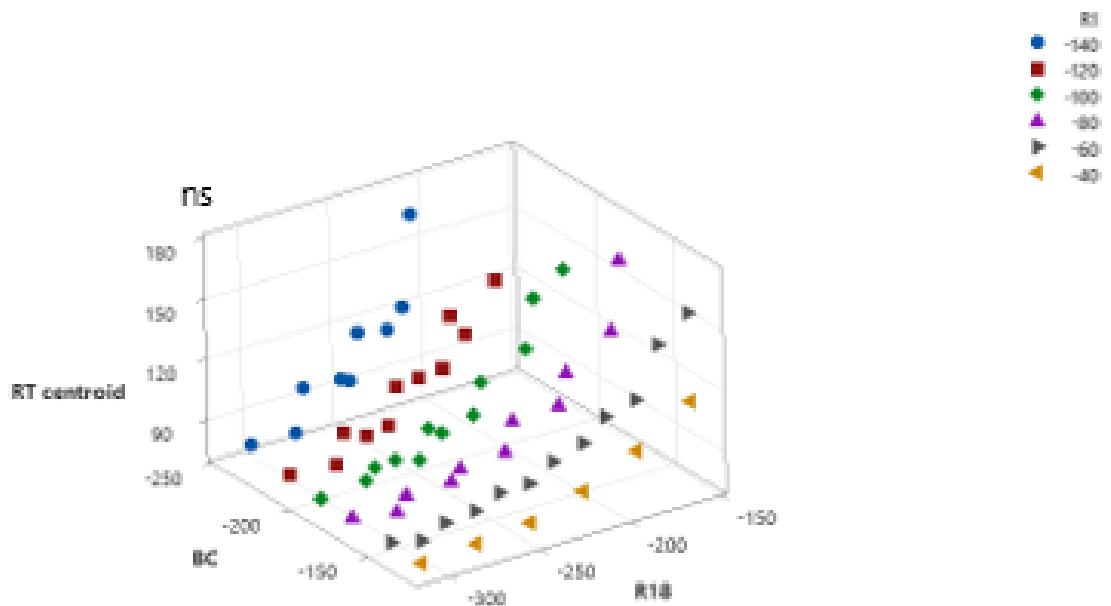
Figure 19. 06_PASS risetime measurements
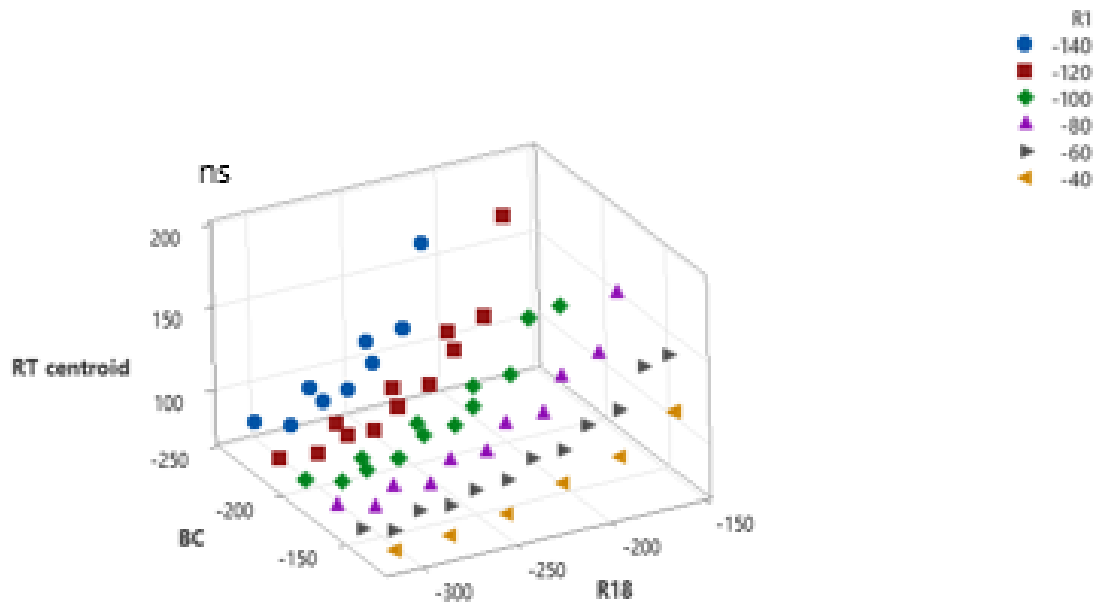
Figure 20. 06_FAIL risetime measurements
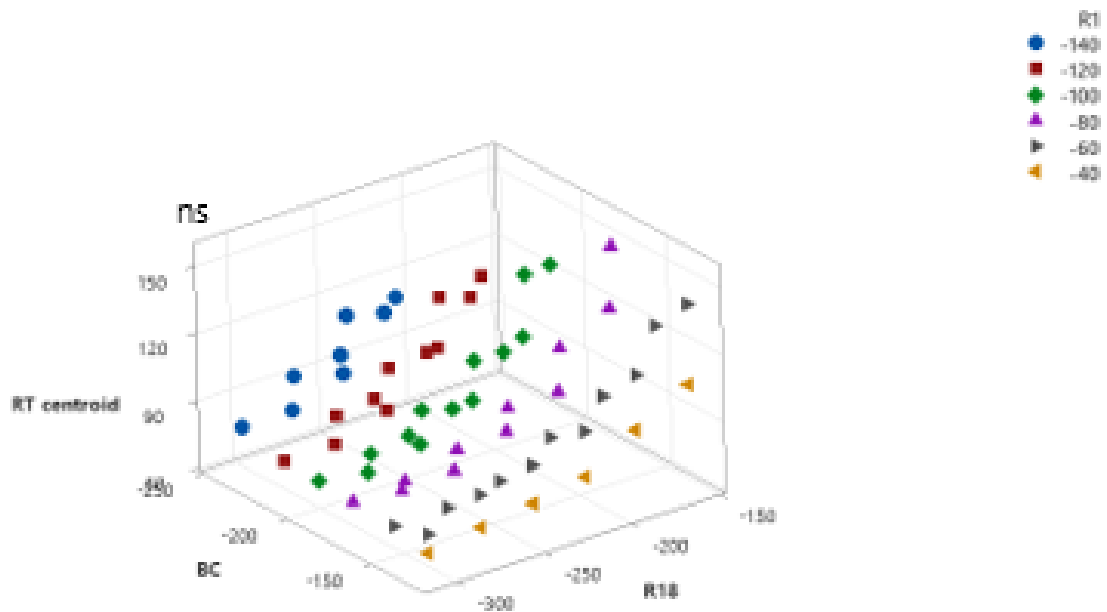
Figure 21. 02_FAIL risetime measurements

As the figures show, risetime behaves similarly in each measured detector. The lowest value for a given R1 is with the highest R18 and BC voltages. Also, as R1 approaches 0 so does risetime, although the effect is not as big as R18 and BC.

5.4 Optimal Bias Voltage Settings

The lowest values of FWHM and risetime occurred with different biasing, so to optimize performance some compromises must be made. To visualise the differences between the three a series of 4 figures each can be seen in figures 22, 23 and 24.
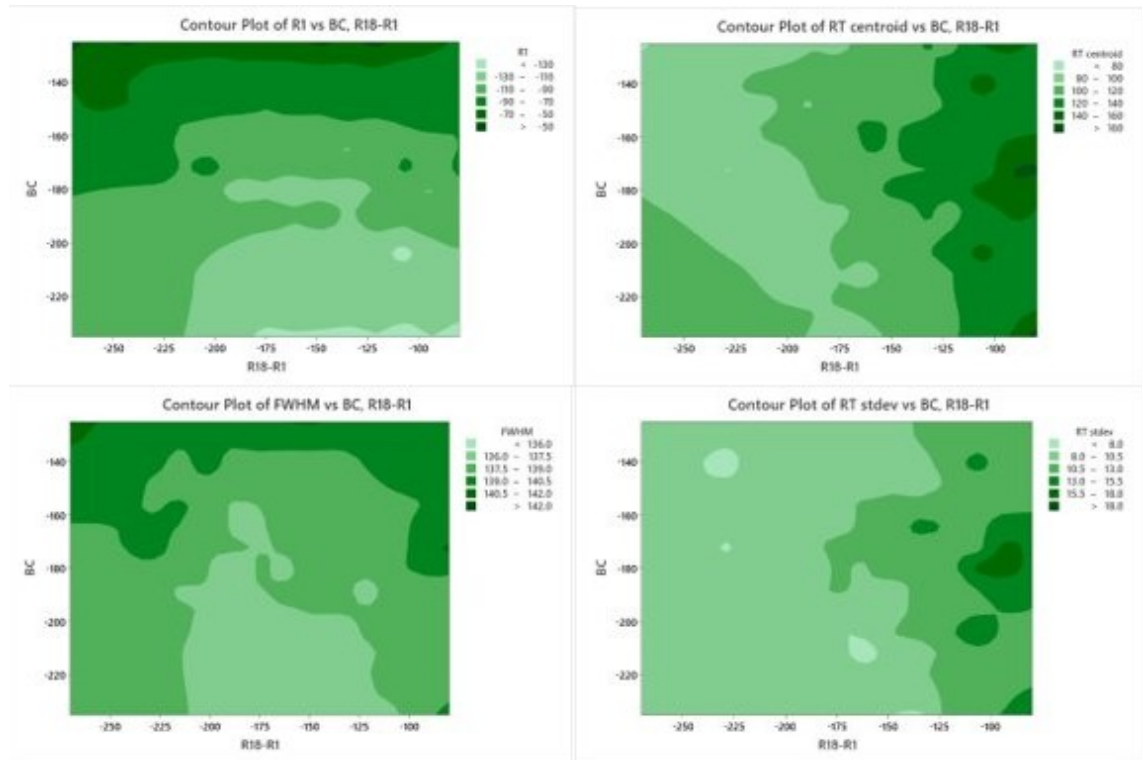
Figure 22. 06_PASS results contour plots for R1 values top left, FWHM bottom left, risetime centroid top right and risetime standard deviation bottom right.
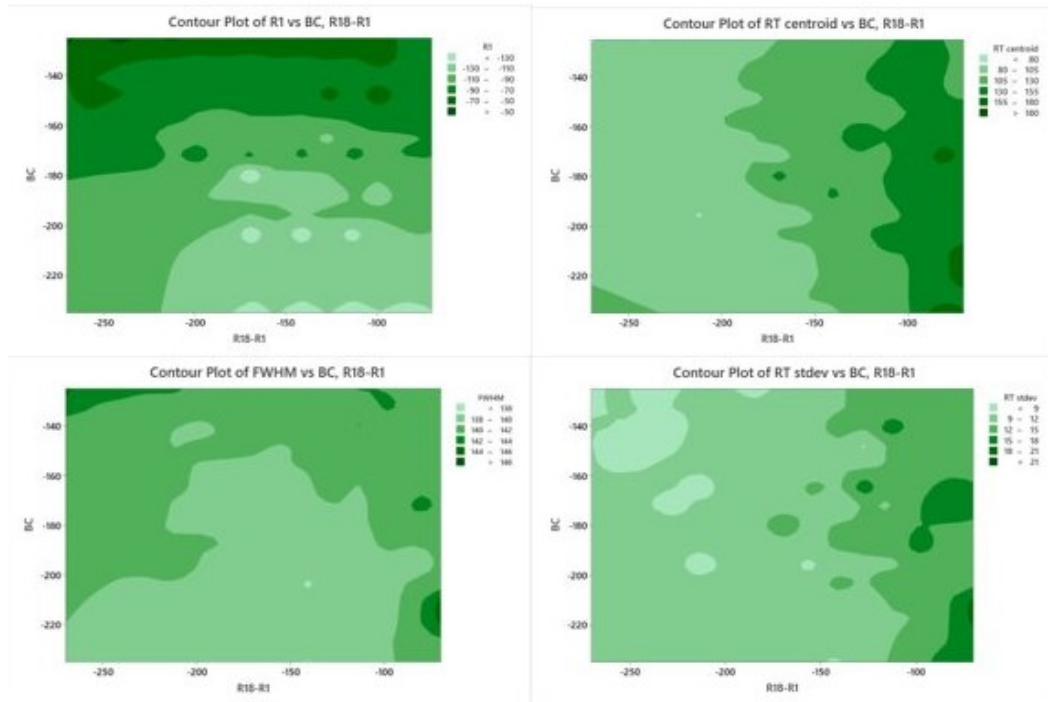
Figure 23. 06_FAIL results contour plots for R1 values top left, FWHM bottom left, risetime centroid top right and risetime standard deviation bottom right.
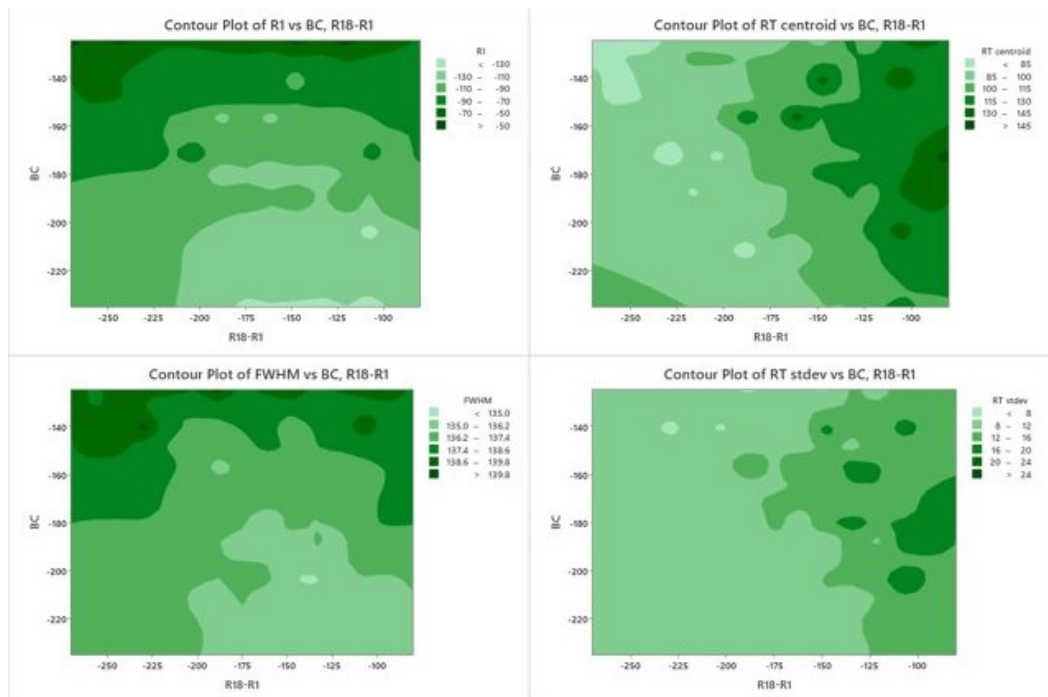
Figure 24. 02_FAIL results contour plots for R1 values top left, FWHM bottom left, risetime centroid top right and risetime standard deviation bottom right.

The top left figure in the series shows R1 values with BC at the Y-axis and the difference between R1 and R18 on X-axis. The R1 values are in the same positions in the three other figures to help visualise the results. The R18 value of a position can be calculated by checking the R1 value and adding it to the X-axis position.

Reviewing all the measurement figures shows that for BC, the optimal voltage is always at the high end of the measurement range for both FWHM and risetime.

Figures 22, 23 and 24 show that the R1-R18 difference should be as large as possible to optimise risetime, but for FWHM the best range is below 200V. For both FWHM and risetime to be as low as possible the R1-R18 difference should be 150V-200V.

Comparing the figures shows that the largest area of optimised performance is with R1 values -120V and -140V.

So, to optimise SDD performance the bias voltages should be set to R1 = 120V–140V, R18= 270V–340V, BC = 240V–220V. Lower R18 would results in better FWHM values but comparing the FWHM and risetime centroid figure shows that risetime increases more rapidly that FWHM decreases. Lower R1 voltages would also improve risetime, but not enough to justify the increase in FWHM.

6 Conclusions

The results show that all the detectors, both ones that are outside the production parameters and the one inside, behave similarly during the adjustments. The edges of the area where the spectrum shape is constant also break in the same way. To improve the optimal bias voltage accuracy more measurements could be made with a smaller step between measurements, but it would be very time intensive, and value added would be minimal.

Another way to improve the results would be to measure with crystals from another batch. All but three detectors measured used silicon crystals from same manufacturing batch, and the three others had worse results than the rest, so it is unlikely that they are indicative of the overall quality of the batch. In the same vein only one type of detector was measured so it is unknown if the behaviour remains consistent with other detector types.

Similar measurements have also been done in two other locations in Japan, once with similar results and once with conflicting results. However, the measurement setup in Espoo was different than in either of the Japanese locations. A copy of the measurement setup in Espoo is being built in Japan to rectify this.

One of the reasons for the project was to explore the need for an automatic solution for sweeping through the many possible bias voltages to find optimal settings. Thanks to the similar optimal ranges in all measured detector, these results do not show the need for an expensive automated solution.

In conclusion, adjusting the bias voltages in a silicon drift detector influences the FWHM and risetime of Fe-55 spectrum but does not influence the low energy tail of the Mn Kα-peak.

References

1   Schlotz, Reinhold; Uhlig Stefan. 2006. Introduction to XRF. Online source. Bruker. http://www.fem.unicamp.br/~liqcqits/facilities/xrf/%5BBruker_2006%5D%20Introduction%20to%20X-ray%20Fluorescence%20(XRF).pdf. Read 26.8.2022

2   Kroneld, Mikael. 2022. Component Development Manager. Hitachi High-tech Analytical Science Finland, Espoo. Lecture. 11.1.2022.

3   Intorduction to Energy Dispersive X-ray Spectrometry (EDS). Online source. Chalmers. http://fy.chalmers.se/~f10mh/Halvarsson/EM_intro_course_files/EDX%20intro%202.pdf. Read 26.8.2022.

4   Chu, S.Y.F; Ekström, L.P; Firestone, R.P. WWW Table of Radioactive isotopes. 1999. Online source. Lund/LBNL Nuclear Data Search. http://nucleardata.nuclear.lu.se/toi/nuclide.asp?iza=260055. Read 26.8.2022

5   Gunell, Jan. 2022. Senior Mechanical Engineer. Hitachi High-tech Analytical Science Finland, Espoo. Lecture. 1.3.2022

6   Silicon Drift Detectors Explained. Online source. Oxford Instruments. https://www.exvil.lt/wp-content/uploads/2012/04/SDD_Explained.pdf. Read 26.8.2022

7   Knoll, Glenn F. 2010. Radiation Detection and Measurement 4th ed. Wiley.

8   Siren, Esko. 2022. Detector Development Engineer. Hitachi High-tech Analytical Science Finland, Espoo. Lecture. 25.1.2022

9   Shaik, Muskan. Depletion region. Online source. Physics and Radio Electronics. https://www.physics-and-radio-electronics.com/electronic-devices-and-circuits/semiconductor-diodes/depletion-region.html. Read 26.8.2022

10   Kairus, Jaakko. 2022. Electronics Design Engineer. Hitachi High-tech Analytical Science Finland, Espoo. Lecture. 15.2.2022.

11   Kemppainen, Jarmo. Process Development Engineer. Hitachi High-tech Analytical Science Finland, Espoo. Lecture. 8.3.2022.

12   Rise time. Online source. Pico Technology. https://www.picotech.com/library/oscilloscopes/rise-time. Read 26.8.2022

Tables of results

Type	S/N	R1	R18	BC	FWHM	Mn tail	RT centroid	RT stdev
4231	72040805	-120	-250	-235	143.4	0.08	97.998	7.701
		-120	-250	-220	142.1	0.08	99.492	8.770
		-120	-250	-205	143.3	0.08	106.236	9.850
		-120	-250	-190	143.1	0.08	117.515	12.251
		-120	-250	-175	144.4	0.09	135.129	15.530
		-120	-250	-160	148.1	0.09	157.613	17.202
		-120	-250	-155	154	0.09	176.700	19.532
		-120	-275	-235	142	0.08	84.958	10.654
		-120	-275	-220	141.5	0.08	86.032	10.585
		-120	-275	-205	142.8	0.08	97.403	8.703
		-120	-275	-190	142.8	0.08	103.570	7.545
		-120	-275	-175	143.2	0.09	116.644	12.321
		-120	-275	-160	145	0.09	114.198	12.903
		-120	-275	-155	146	0.09	153.656	13.181
		-120	-290	-235	163.9	0.13	77.816	7.729
		-120	-290	-220	140.8	0.08	81.026	9.639
		-120	-290	-205	141.5	0.08	87.483	10.437
		-120	-290	-190	142.7	0.08	102.180	7.336
		-120	-290	-175	144.4	0.08	113.446	12.164
		-120	-290	-160	144.2	0.09	134.537	12.046
		-120	-305	-235	167.5	0.16	75.836	7.439
		-120	-305	-220	141.1	0.08	78.265	8.191
		-120	-305	-205	140.5	0.09	81.118	9.635
		-120	-305	-190	141.8	0.08	92.873	7.117
		-120	-305	-175	143.9	0.08	105.437	8.213
		-120	-305	-160	144.3	0.09	130.410	11.508
		-120	-305	-155	143.9	0.09	140.654	10.854
		-120	-235	-235	141.4	0.08	107.863	8.038
		-120	-235	-220	142.5	0.08	108.103	8.922
		-120	-235	-205	142.8	0.08	118.025	11.774
		-120	-235	-190	143.2	0.08	128.605	12.524
		-120	-235	-175	147.7	0.09	148.810	17.333
		-120	-235	-160	158.9	0.09	180.101	21.277
		-120	-220	-235	145.4	0.08	113.740	9.667
		-120	-220	-220	142.7	0.09	115.563	10.461
		-120	-220	-205	143.3	0.08	124.018	12.987
		-120	-220	-190	145.6	0.09	143.279	15.851
		-120	-220	-175	155.3	0.09	173.983	20.476
		-120	-220	-160	176.4	0.11	203.034	27.711
		-120	-205	-235	144.2	0.09	132.708	9.361

Type	S/N	R1	R18	BC	FWHM	Mn tail	RT centroid	RT stdev
		-120	-205	-220	143.9	0.08	133.515	11.673
		-120	-205	-205	145.5	0.09	145.189	13.795
		-120	-205	-190	155.5	0.09	170.590	20.417
		-120	-205	-175	174	0.12	194.253	25.536
		-120	-190	-235	148.4	0.09	158.552	14.356
		-120	-190	-220	150.8	0.09	162.442	15.45
		-120	-190	-205	164.8	0.1	182.526	21.982
		-120	-190	-190	188.3	0.14	207.825	30.613
		-120	-175	-235	177.3	0.11	205.480	20.399
4231	72030508	-120	-310	-235	160.4	0.1	76.099	7.692
		-120	-310	-205	156.3	0.1	82.075	10.991
		-120	-310	-175	157.3	0.1	105.497	9.802
		-120	-310	-165	158.4	0.1	118.362	14.758
		-120	-280	-235	169.3	0.97	85.639	11.566
		-120	-280	-205	155.8	0.1	94.176	7.009
		-120	-280	-175	157.8	0.1	119.206	13.880
		-120	-280	-165	159.7	0.1	132.818	16.776
		-120	-250	-225	155.9	0.09	102.501	6.723
		-120	-250	-195	156.3	0.1	111.794	12.281
		-120	-250	-165	162.7	0.11	150.700	19.251
		-120	-220	-225	155.9	0.1	119.305	11.699
		-120	-220	-195	159.2	0.1	135.143	19.277
		-120	-220	-165	185.1	0.18	185.452	32.936
		-120	-190	-225	169.7	0.11	177.194	17.641
		-120	-190	-195	199.4	0.23	193.767	36.046
		-120	-190	-185	243.3	0.44	210.729	42.162
		-140	-310	-235	155.9	0.1	88.075	10.184
		-140	-310	-205	158.4	0.1	108.335	12.372
		-140	-310	-175	164.9	0.11	165.400	17.362
		-140	-280	-235	155.9	0.1	101.616	8.061
		-140	-280	-205	158.8	0.1	119.037	16.020
		-140	-280	-175	172.6	0.12	181.104	23.487
		-140	-250	-235	158.9	0.1	123.089	14.396
		-140	-250	-205	161.2	0.11	139.795	22.909
		-140	-250	-175	208.6	0.32	210.790	37.563
		-140	-220	-235	171	0.12	169.041	19.912
		-140	-220	-205	219.1	0.37	194.143	41.648
		-100	-310	-215	167.2	0.11	75.868	7.520
		-100	-310	-185	156.7	0.1	84.700	11.171
		-100	-310	-170	156.9	0.1	93.168	7.533
		-100	-280	-215	177.8	0.62	83.181	10.211
		-100	-280	-185	155.3	0.1	89.586	9.268
		-100	-280	-170	155.9	0.1	97.330	9.133
		-100	-250	-210	154.3	0.09	86.901	10.896

		R1	R18	BC	FWHM	Mn tail	RT centroid	RT stdev
		-100	-250	-185	155	0.09	96.655	8.700
		-100	-250	-170	155.5	0.1	106.312	9.246
		-100	-250	-160	157.9	0.1	119.205	12.861
		-100	-250	-150	158.9	0.1	127.668	14.688
		-100	-250	-140	164	0.11	163.595	17.082
		-100	-220	-210	156.5	0.1	108.900	9.210
		-100	-220	-185	157.3	0.1	118.577	11.333
		-100	-220	-160	158.4	0.1	134.516	15.012
		-100	-220	-140	165.8	0.1	164.644	23.440
		-100	-190	-210	159.1	0.1	143.011	9.628
		-100	-190	-180	161.7	0.1	160.634	15.021
		-100	-190	-160	171.4	0.11	173.868	25.549
		-100	-170	-200	165.1	0.1	164.550	17.598
		-80	-310	-190	155.7	0.1	74.864	7.257
		-80	-310	-160	154.6	0.1	81.253	9.972
		-80	-310	-130	156.8	0.1	106.288	7.578
		-80	-280	-190	154.5	0.09	78.601	7.805
		-80	-280	-160	153.8	0.09	84.216	10.470
		-80	-280	-130	158.1	0.1	117.714	11.714
		-80	-250	-185	154.4	0.1	79.671	9.003
		-80	-250	-155	154.6	0.1	93.940	6.694
		-80	-250	-125	158.6	0.1	129.737	12.271
		-80	-220	-190	179	0.2	92.514	6.690
		-80	-220	-160	156	0.1	102.724	7.623
		-80	-220	-130	158.7	0.1	131.817	13.287
		-80	-190	-185	155.1	0.1	109.903	8.843
		-80	-190	-155	156.7	0.1	123.216	12.967
		-80	-190	-125	167.7	0.11	175.320	19.520
		-80	-170	-185	156.6	0.09	124.772	10.394
		-80	-170	-155	157.8	0.1	141.379	12.838
		-80	-170	-135	169.2	0.11	174.162	22.440
Type	S/N	R1	R18	BC	FWHM	Mn tail	RT centroid	RT stdev
4231	72020207	-140	-310	-235	148.2	0.09	88.821	9.989
		-140	-310	-205	146.9	0.08	102.739	8.484
		-140	-310	-175	148.5	0.08	138.255	12.485
		-140	-280	-235	147.7	0.09	95.716	7.794
		-140	-280	-205	147.4	0.08	115.575	13.07
		-140	-280	-180	150	0.09	145.146	15.772
		-140	-250	-240	148.2	0.09	111.331	10.467
		-140	-250	-210	150.2	0.09	135.775	14.415
		-140	-250	-190	156.7	0.12	158.943	18.994
		-140	-220	-240	155.7	0.12	158.603	15.386
		-140	-220	-210	173.5	0.18	178.772	24.238
		-120	-310	-220	147.4	0.09	77.854	8.457
		-120	-310	-190	148.1	0.08	92.959	7.131

-120	-310	-160	147.8	0.08	115.981	11.916
-120	-280	-220	147.5	0.09	89.122	9.215
-120	-280	-190	148.1	0.08	102.466	7.749
-120	-280	-160	148.9	0.08	135.204	12.134
-120	-250	-220	148.7	0.08	104.786	6.908
-120	-250	-190	148	0.08	119.063	12.811
-120	-250	-165	151.1	0.09	144.199	14.224
-120	-220	-220	150.5	0.09	126.454	11.603
-120	-220	-190	152.3	0.09	143.589	13.986
-120	-190	-220	167.1	0.14	181.251	14.416
-100	-310	-200	147.6	0.08	75.356	7.783
-100	-310	-170	148.1	0.08	86.36	10.976
-100	-310	-145	148.4	0.08	106.893	9.267
-100	-280	-200	148.5	0.08	80.697	9.712
-100	-280	-170	148.3	0.08	95.532	7.867
-100	-280	-145	148.5	0.09	116.126	12.616
-100	-250	-200	148.4	0.08	93.481	6.371
-100	-250	-170	149.5	0.08	104.582	7.898
-100	-250	-145	150.8	0.09	135.258	13.316
-100	-220	-200	149.7	0.08	110.396	9.24
-100	-220	-170	150.4	0.08	125.25	13.254
-100	-220	-150	152.9	0.09	145.362	15.06
-100	-190	-200	153.5	0.09	136.646	11.952
-100	-190	-175	155	0.09	148.292	15.783
-80	-310	-180	150.7	0.09	74.384	7.62
-80	-310	-150	150	0.08	83.346	11.48
-80	-310	-125	150	0.08	107.691	8.937
-80	-280	-180	150.4	0.08	79.712	9.206
-80	-280	-150	149.3	0.09	88.971	9.683
-80	-280	-130	150.6	0.09	105.734	7.489
-80	-250	-180	150.2	0.08	84.203	10.288
-80	-250	-150	149.3	0.08	99.723	8.973
-80	-250	-130	149.7	0.09	114.238	11.532
-80	-220	-175	150.6	0.09	94.802	7.441
-80	-220	-145	149.4	0.09	111.743	11
-80	-220	-125	154	0.09	147.448	14.235
-80	-190	-180	152.3	0.08	113.775	10.416
-80	-190	-150	152	0.09	131.884	11.784
-80	-160	-180	158.4	0.11	156.605	14.071
-80	-160	-165	157.9	0.18	157.199	15.341
-60	-310	-155	152.1	0.09	74.885	7.586
-60	-310	-125	151	0.09	83.451	11.123
-60	-280	-160	151.1	0.09	74.833	7.794
-60	-280	-130	150.1	0.09	85.123	10.27
-60	-250	-155	151.8	0.09	79.286	8.744

Type	S/N	R1	R18	BC	FWHM	Mn tail	RT centroid	RT stdev
		-60	-250	-125	151.5	0.09	95.089	7.163
		-60	-220	-155	151	0.09	85.367	11.048
		-60	-220	-120	152	0.09	105.203	7.818
		-60	-190	-155	152.6	0.09	102.398	6.628
		-60	-190	-125	152.8	0.09	117.943	12.535
		-60	-160	-155	154.4	0.09	122.119	11.374
		-60	-160	-130	155.8	0.09	144.483	13.665
		-40	-310	-130	153.8	0.09	70.961	8.066
		-40	-280	-130	153.5	0.09	74.052	7.652
		-40	-250	-135	154.5	0.09	77.277	7.592
		-40	-220	-135	154.5	0.09	83.371	10.74
		-40	-190	-135	155.2	0.09	91.568	7.542
		-40	-160	-135	156.6	0.09	104.379	7.067
8525	72020608	-140	-310	-235	136.3	0.08	80.683	10.352
icr 59k	dt 17%	-140	-310	-205	137.9	0.08	100.165	9.671
		-140	-310	-175	140.4	0.09	135.639	15.879
		-140	-280	-235	136.7	0.08	97.385	8.626
		-140	-280	-205	137.1	0.09	110.057	13.015
		-140	-280	-180	138.5	0.09	139.322	18.643
		-140	-250	-235	136.8	0.09	114.017	13.289
		-140	-250	-205	138.2	0.09	136.601	20.13
		-140	-250	-185	140.5	0.09	162.654	23.872
		-140	-220	-235	140.4	0.08	158.715	19.984
		-140	-220	-205	146.5	0.1	183.031	28.438
		-120	-310	-215	137.3	0.09	78.32	8.668
		-120	-310	-185	140.3	0.09	97.495	10.088
		-120	-310	-160	139.3	0.09	120.412	14.442
		-120	-280	-215	137.8	0.08	85.332	11.605
		-120	-280	-185	138.2	0.08	104.519	8.484
		-120	-280	-160	139	0.09	135.991	14.067
		-120	-250	-215	138.5	0.09	104.15	7.729
		-120	-250	-185	138.8	0.09	118.747	15.02
		-120	-250	-165	139.6	0.09	145.764	17.082
		-120	-220	-215	139.1	0.08	134.209	13.273
		-120	-220	-185	139.6	0.09	146.652	19.65
		-120	-190	-215	144	0.09	182.718	22.558
		-100	-310	-195	139.1	0.09	76.365	7.567
		-100	-310	-165	139.8	0.09	90.912	8.981
		-100	-310	-145	139.7	0.09	107.751	10.703
		-100	-280	-195	137.7	0.08	82.638	10.687
		-100	-280	-165	138.3	0.08	97.634	9.763
		-100	-280	-145	137.9	0.09	114.047	12.028
		-100	-250	-195	137.2	0.08	93.878	6.456
		-100	-250	-165	138.4	0.09	108.105	11.955

Type	S/N	R1	R18	BC	FWHM	Mn tail	RT centroid	RT stdev
		-100	-250	-145	139.6	0.09	134.08	14.091
		-100	-220	-195	138.5	0.08	110.741	10.364
		-100	-220	-165	138.2	0.09	125.545	14.333
		-100	-220	-150	138.7	0.09	141.408	19.06
		-100	-190	-195	137.7	0.09	132.524	13.362
		-100	-190	-165	140.2	0.1	155.237	22.078
		-80	-310	-175	141.2	0.09	76.198	7.869
		-80	-310	-145	139.8	0.09	86.829	11.139
		-80	-310	-125	140.6	0.09	107.407	9.103
		-80	-280	-175	139.1	0.09	78.592	7.97
		-80	-280	-145	138.7	0.09	90.986	8.726
		-80	-280	-130	139.2	0.09	103.781	7.753
		-80	-250	-175	138.4	0.09	83.68	10.916
		-80	-250	-145	140	0.08	101.536	8.719
		-80	-250	-130	140.3	0.09	117.212	13.415
		-80	-220	-175	139.2	0.08	96.663	8.906
		-80	-220	-145	138.1	0.09	108.293	10.734
		-80	-220	-130	140	0.09	129.125	15.047
		-80	-190	-175	139.4	0.09	112.546	12.297
		-80	-190	-145	140.6	0.09	134.776	15.731
		-80	-190	-130	140.3	0.09	155.515	19.213
		-80	-160	-175	140.1	0.09	150.788	15.739
		-80	-160	-150	141.4	0.09	163.017	20.417
		-60	-310	-150	140.4	0.08	73.314	7.805
		-60	-310	-125	141	0.09	86.522	11.196
		-60	-280	-150	139.6	0.09	78.329	8.506
		-60	-280	-125	141.2	0.09	102.793	8.127
		-60	-250	-150	139.4	0.09	78.734	8.629
		-60	-250	-125	141	0.09	97.91	9.619
		-60	-220	-150	139.6	0.08	88.234	10.504
		-60	-220	-125	140.6	0.09	107.227	9.458
		-60	-190	-155	140.1	0.09	98.406	8.784
		-60	-190	-125	141.3	0.09	121.076	14.217
		-60	-160	-155	139.9	0.08	122.429	11.933
		-60	-160	-125	140.5	0.09	143.137	14.809
		-40	-310	-130	141.8	0.09	72.746	7.747
		-40	-280	-130	141	0.09	75.155	8.288
		-40	-250	-130	140.3	0.09	77.198	7.704
		-40	-220	-130	140.3	0.09	82.118	10.094
		-40	-190	-135	140.8	0.08	91.545	7.769
		-40	-160	-135	140.1	0.09	103.516	7.57
8525	72030608	-140	-310	-245	139.4	0.08	96.559	8.843
icr 63k	dt 18%	-140	-310	-215	141.4	0.09	118.202	13.653
		-140	-310	-185	143	0.09	154.361	19.931

-140	-280	-245	138	0.08	111.027	10.292
-140	-280	-215	138.8	0.08	129.911	16.336
-140	-280	-200	142.4	0.15	146.579	16.58
-140	-250	-245	139.8	0.08	144.506	12.86
-140	-250	-215	143	0.09	163.589	22.883
-140	-220	-240	147.1	0.09	197.314	26.72
-120	-310	-225	139.3	0.08	86.52	11.16
-120	-310	-195	143.5	0.09	107.068	9.521
-120	-310	-165	141.9	0.09	142.283	17.537
-120	-280	-225	138.5	0.08	103.18	7.691
-120	-280	-195	140.5	0.09	119.693	14.379
-120	-280	-175	140.4	0.09	137.217	15.15
-120	-250	-225	137.5	0.08	115.85	10.478
-120	-250	-195	141.5	0.09	142.049	17.092
-120	-220	-225	139.9	0.08	152.801	15.527
-120	-220	-210	139.9	0.08	153.421	22.342
-100	-310	-200	142.4	0.09	87.18	11.567
-100	-310	-170	143.1	0.1	101.992	8.79
-100	-310	-145	138.9	0.09	128.019	15.866
-100	-280	-200	138.4	0.08	92.457	7.253
-100	-280	-170	140	0.1	108.362	10.504
-100	-280	-150	141.6	0.09	135.679	14.352
-100	-250	-200	139.6	0.08	105.442	8.337
-100	-250	-170	142	0.1	129.192	14.346
-100	-220	-200	139.4	0.08	124.308	14.538
-100	-220	-175	141	0.09	147.488	17.245
-100	-190	-200	139.6	0.08	157.19	18.775
-80	-310	-180	142.6	0.09	81.596	10.611
-80	-310	-150	141.7	0.09	95.872	7.514
-80	-310	-130	140.5	0.08	115.147	12.845
-80	-280	-180	139.9	0.08	85.246	11.316
-80	-280	-150	143	0.09	104.509	8.15
-80	-280	-130	141.3	0.09	127.581	14.791
-80	-250	-180	139.9	0.08	95.747	7.628
-80	-250	-150	142	0.1	112.931	11.348
-80	-250	-135	141.9	0.09	132.558	14.596
-80	-220	-180	139.3	0.08	104.89	8.314
-80	-220	-150	142.3	0.1	135.04	14.475
-80	-190	-180	139.8	0.08	132.194	13.706
-80	-190	-155	143.8	0.09	157.142	20.379
-80	-160	-185	143.4	0.09	176.189	18.885
-60	-310	-160	143.7	0.09	79.667	9.135
-60	-310	-130	143.9	0.09	96.253	8.602
-60	-280	-160	141.9	0.09	81.55	10.343
-60	-280	-130	144.3	0.09	101.638	8.163

Type	S/N	R1	R18	BC	FWHM	Mn tail	RT centroid	RT stdev
		-60	-250	-160	140.6	0.08	87.377	10.624
		-60	-250	-130	143	0.1	107.816	9.355
		-60	-220	-160	140.7	0.08	97.434	8.3
		-60	-220	-130	142.3	0.09	118.42	12.322
		-60	-190	-160	140.8	0.08	110.01	10.566
		-60	-190	-130	144.4	0.11	144.788	16.157
		-60	-160	-160	141.8	0.09	141.151	12.129
		-60	-160	-140	143.9	0.09	158.936	19.832
		-40	-310	-135	142.7	0.09	77.53	7.138
		-40	-280	-135	142.4	0.09	78.984	8.471
		-40	-250	-135	141.7	0.09	83.216	10.92
		-40	-220	-135	141.7	0.09	92.125	7.552
		-40	-190	-140	142.3	0.08	98.298	8.738
		-40	-160	-140	142.1	0.09	115.004	11.044
Type	S/N	R1	R18	BC	FWHM	Mn tail	RT centroid	RT stdev
4231	72040804	-140	-310	-245	140.3	0.09	82.765	10.316
icr 60k		-140	-310	-215	140.4	0.09	95.42	7.94
		-140	-310	-185	141.8	0.09	123.958	13.253
		-140	-280	-245	141.6	0.09	96.64	8.029
		-140	-280	-215	142	0.09	107.629	9.984
		-140	-280	-185	145.1	0.09	146.045	15.841
		-140	-250	-245	142.4	0.09	117.86	11.469
		-140	-250	-215	142.3	0.09	132.241	13.184
		-120	-310	-220	140.4	0.09	78.095	8.035
		-120	-310	-190	142.6	0.09	97.399	8.964
		-120	-310	-165	143.2	0.09	116.844	11.347
		-120	-280	-220	141.6	0.09	88.537	9.681
		-120	-280	-190	142.8	0.09	103.028	7.255
		-120	-280	-165	142.5	0.09	126.447	11.998
		-120	-250	-220	141.4	0.09	100.202	8.395
		-120	-250	-190	143.6	0.09	122.264	11.977
		-120	-250	-165	146	0.09	149.93	14.343
		-120	-220	-220	142.6	0.09	123.967	10.232
		-120	-220	-190	146.8	0.09	152.167	15.39
		-100	-310	-200	143.4	0.09	76.906	7.43
		-100	-310	-170	143.5	0.09	89.783	9.336
		-100	-310	-145	143.1	0.09	112.461	10.039
		-100	-280	-200	143	0.09	79.992	9.604
		-100	-280	-170	142.2	0.09	93.902	6.705
		-100	-280	-145	144.3	0.09	126.449	12.244
		-100	-250	-200	142.9	0.09	91.907	7.086
		-100	-250	-170	142.8	0.09	105.721	7.674
		-100	-250	-150	144.8	0.09	134.817	9.613
		-100	-220	-200	143.3	0.09	107.979	8.652
		-100	-220	-170	143	0.09	124.144	11.292

Type	S/N	R1	R18	BC	FWHM	Mn tail	RT centroid	RT stdev
		-100	-220	-150	147.6	0.1	156.012	15.088
		-100	-190	-200	145.1	0.09	140.127	10.627
		-100	-190	-170	149.3	0.09	160.793	15.908
		-80	-310	-180	144.8	0.09	76.718	7.413
		-80	-310	-150	145.7	0.09	90.079	9.247
		-80	-310	-130	144.5	0.1	100.858	7.619
		-80	-280	-180	143.5	0.09	76.93	7.369
		-80	-280	-150	144.2	0.09	93.114	6.449
		-80	-280	-130	144.8	0.09	108.774	8.868
		-80	-250	-180	144.1	0.09	81.369	9.736
		-80	-250	-150	144.9	0.09	101.842	7.154
		-80	-250	-130	144.7	0.09	119.381	10.6
		-80	-220	-180	143.6	0.09	92.667	6.645
		-80	-220	-150	145.1	0.09	113.939	8.951
		-80	-220	-130	145.9	0.1	138.737	10.66
		-80	-190	-180	145	0.09	110.431	9.484
		-80	-190	-150	146.7	0.09	139.305	11.761
		-80	-160	-180	149.2	0.09	155.536	13.434
		-60	-310	-155	145.5	0.09	74.242	7.648
		-60	-310	-125	146.2	0.09	89.635	9.357
		-60	-280	-155	144.5	0.09	74.838	7.559
		-60	-280	-125	145.9	0.09	93.037	6.554
		-60	-250	-155	146	0.09	80.832	10.17
		-60	-250	-125	147	0.09	101.471	7.276
		-60	-220	-155	144.8	0.09	88.579	9.35
		-60	-220	-125	145.9	0.09	109.227	9.039
		-60	-190	-155	145.5	0.09	98.905	8.772
		-60	-190	-125	147.9	0.09	131.047	10.651
		-60	-160	-155	147.7	0.09	126.461	11.48
		-60	-160	-125	149.1	0.09	153.291	12.764
		-40	-310	-130	148	0.09	73.157	7.525
		-40	-280	-130	146.8	0.09	75.277	7.376
		-40	-250	-130	147.9	0.1	78.496	7.907
		-40	-220	-130	148.5	0.09	88.855	9.54
		-40	-190	-130	147.5	0.1	95.044	6.302
		-40	-160	-130	150.1	0.09	116.516	10.351
Type	S/N	R1	R18	BC	FWHM	Mn tail	RT centroid	RT stdev
4231	72020308	-140	-310	-235	142.9	0.09	86.298	10.421
		-140	-310	-205	144.4	0.09	102.578	7.562
		-140	-310	-175	147.6	0.1	144.787	15.797
		-140	-280	-230	143.2	0.09	100.909	8.107
		-140	-280	-200	144.8	0.09	122.886	13.746
		-140	-280	-185	149.3	0.1	148.02	19.255
		-140	-250	-230	145.1	0.09	123.659	15.007
		-140	-250	-200	150	0.09	147.396	20.205

-140	-220	-230	161.6	0.11	169.431	22.083
-120	-310	-210	143.4	0.09	77.931	8.768
-120	-310	-180	146.4	0.09	102.749	8.355
-120	-310	-155	145.1	0.09	131.986	12.483
-120	-280	-210	144.7	0.09	92.432	6.67
-120	-280	-180	145.2	0.09	109.723	11.25
-120	-280	-160	148.4	0.1	141.429	14.235
-120	-250	-210	144.4	0.09	104.377	8.151
-120	-250	-180	146.9	0.09	132.316	13.06
-120	-220	-210	146	0.09	128.965	13.752
-120	-220	-190	152.2	0.09	151.34	19.027
-100	-310	-190	145.9	0.09	78.105	8.46
-100	-310	-160	145.4	0.09	96.015	7.928
-100	-310	-135	146.5	0.09	118.799	11.835
-100	-280	-190	145.1	0.09	80.983	9.705
-100	-280	-160	146.3	0.09	102.518	7.805
-100	-280	-140	146	0.1	124.722	13.456
-100	-250	-190	145.1	0.09	94.945	7.104
-100	-250	-160	145.9	0.09	116.095	11.817
-100	-250	-140	150.2	0.09	148.023	16.609
-100	-220	-190	146	0.09	109.254	11.252
-100	-220	-160	147.7	0.09	137.497	13.094
-100	-190	-190	150.1	0.09	145.833	14.749
-100	-190	-175	154.1	0.1	157.072	18.739
-80	-310	-170	146.3	0.09	76.522	7.461
-80	-310	-140	146.2	0.09	87.897	10.725
-80	-310	-125	148.4	0.09	106.221	8.853
-80	-280	-170	146.9	0.1	77.317	8.462
-80	-280	-140	146.9	0.09	93.908	6.795
-80	-280	-125	147.3	0.09	110.662	10.565
-80	-250	-170	146.2	0.09	86.816	10.707
-80	-250	-140	147.3	0.1	105.282	8.072
-80	-250	-125	147.6	0.09	123.675	13.139
-80	-220	-170	146.7	0.09	97.287	8.677
-80	-220	-140	148.6	0.09	122.478	12.16
-80	-190	-170	148.4	0.09	121.523	11.005
-80	-190	-140	150	0.09	145.418	14.844
-80	-160	-170	153.6	0.1	152.713	16.683
-60	-310	-150	148.1	0.09	73.705	7.667
-60	-310	-125	148.4	0.1	81.064	10.193
-60	-280	-150	147.5	0.09	77.054	8.343
-60	-280	-125	148.2	0.09	87.14	10.616
-60	-250	-150	147.7	0.09	79.887	9.272
-60	-250	-125	148.9	0.09	96.32	8.169
-60	-220	-150	148	0.09	85.879	11.021

Type	S/N	R1	R18	BC	FWHM	Mn tail	RT centroid	RT stdev
		-60	-220	-125	149.2	0.1	105.076	7.954
		-60	-190	-150	149.6	0.09	102.898	7.22
		-60	-190	-125	149.7	0.1	119.846	12.088
		-60	-160	-150	149.6	0.09	122.407	12.031
		-60	-160	-125	154.1	0.1	154.607	16.521
		-40	-310	-125	151.4	0.1	74.372	8.173
		-40	-340	-125	150.9	0.1	72.84	7.553
		-40	-370	-125	150.5	0.1	69.859	7.694
		-40	-400	-125	151.3	0.1	70.111	7.832
		-40	-280	-125	149.4	0.1	77.453	7.837
		-40	-250	-125	150.9	0.09	84.708	10.958
		-40	-220	-125	149.9	0.09	89.98	8.719
		-40	-190	-125	151.3	0.1	104.074	6.348
		-40	-160	-125	151.8	0.1	117.821	11.789
Type	S/N	R1	R18	BC	FWHM	Mn tail	RT centroid	RT stdev
8525	75040105	-140	-310	-310	140.3	0.05	143.067	10.484
63 cps		-140	-280	-315	141.3	0.05	152.763	14.51
dt 19%		-120	-310	-285	140.5	0.05	112.667	12.407
		-120	-310	-270	140.5	0.05	137.279	16.703
		-120	-280	-285	141.8	0.05	148.128	11.343
		-100	-310	-260	143.7	0.05	112.115	13.04
		-100	-310	-235	142.3	0.05	147.384	19.837
		-100	-280	-260	140.5	0.05	130.718	13.958
		-100	-250	-265	144.5	0.05	160.386	18.265
		-80	-310	-240	142.4	0.05	100.632	9.271
		-80	-310	-210	141.7	0.05	138.581	15.001
		-80	-280	-240	139.5	0.05	107.313	9.244
		-80	-280	-215	143.6	0.05	159.714	17.706
		-80	-250	-245	141.1	0.05	124.755	15.045
		-60	-310	-220	143.9	0.05	92.252	9.328
		-60	-310	-190	141	0.05	124.906	13.174
		-60	-280	-220	139.9	0.05	97.852	8.946
		-60	-280	-195	143.6	0.05	140.249	12.073
		-60	-250	-220	140.9	0.05	119.147	12.578
		-60	-250	-205	143.7	0.05	151.348	13.128
		-60	-220	-220	143.7	0.05	148.869	12.198
		-40	-310	-195	145.5	0.05	93.695	9.051
		-40	-310	-170	145.7	0.05	126.855	17.739
		-40	-280	-195	143.1	0.05	99.302	9.626
		-40	-280	-175	145.3	0.05	131.801	20.007
		-40	-250	-195	141.5	0.05	106.71	7.934
		-40	-220	-200	144.1	0.05	126.128	12.325
Type	S/N	R1	R18	BC	FWHM	Mn tail	RT centroid	RT stdev
8525	75040106	-140	-310	-275	150	0.08	101.016	13.842

	R1	R18	BC	FWHM	Mn tail	RT centroid	RT stdev
cps 57k	-120	-310	-260	146.9	0.05	92.729	10.573
dt 17%	-120	-280	-260	148.8	0.07	103.078	8.883
	-100	-310	-235	153.6	0.05	95.822	15.292
	-100	-280	-235	147.3	0.05	93.818	11.284
	-80	-310	-215	160.4	0.06	110.779	21.158
	-80	-310	-185	158.6	0.06	115.598	19.422
	-80	-280	-215	155	0.05	101.861	15.003
	-80	-250	-215	151.7	0.06	103.495	11.902
	-60	-310	-195	160.3	0.06	106.569	19.938
	-60	-310	-160	157.6	0.06	113.56	20.035
	-60	-280	-195	153.9	0.05	99	14.464
	-60	-280	-175	161.3	0.06	125.897	31.1
	-60	-250	-195	155.6	0.05	106.579	13.76
	-40	-310	-170	160.1	0.06	102.443	18.95
	-40	-310	-140	161	0.06	124.888	25.501
	-40	-280	-170	161.1	0.06	112.473	21.288
	-40	-280	-140	158	0.06	124.905	23.802
	-40	-250	-170	157.1	0.06	105.855	13.767
	-40	-250	-155	162.5	0.06	136.411	33.498
	-40	-220	-170	158.9	0.06	122.335	23.602

Type	S/N	R1	R18	BC	FWHM	Mn tail	RT centroid	RT stdev
8525	75040103							

Ei hyvää spektriä millään bias arvoilla

Type	S/N	R1	R18	BC	FWHM	Mn tail	RT centroid	RT stdev
4231	72020508	-140	-310	-240	135.8	0.08	83.502	11.208
61kcps		-140	-310	-210	136	0.08	101.246	9.966
17% dt		-140	-310	-180	133.7	0.08	129.706	20.567
		-140	-280	-240	132.1	0.08	94.518	7.308
		-140	-280	-210	133.7	0.08	113.076	14.267
		-140	-280	-190	134.6	0.08	138.388	20.55
		-140	-250	-240	132.6	0.08	111.998	12.064
		-140	-250	-210	134.7	0.08	135.534	18.914
		-140	-220	-235	134.6	0.08	151.284	18.293
		-120	-310	-215	136	0.08	79.084	8.828
		-120	-310	-185	134	0.08	93.931	8.043
		-120	-310	-160	134.7	0.09	120.55	18.891
		-120	-280	-215	132.9	0.08	85.63	10.957
		-120	-280	-185	134.3	0.08	105.193	9.652
		-120	-280	-165	134.2	0.08	127.98	20.125
		-120	-250	-215	132.4	0.08	98.951	9.009
		-120	-250	-185	134.2	0.08	124.467	16.491
		-120	-250	-170	136	0.08	143.921	22.257
		-120	-220	-215	133.7	0.08	119.844	13.52
		-120	-220	-190	135.3	0.08	142.982	19.741

-100	-310	-195	137.4	0.08	77.08	7.866
-100	-310	-165	133.8	0.08	87.765	10.551
-100	-310	-140	135.1	0.08	116.518	16.517
-100	-280	-195	134.1	0.08	80.756	9.751
-100	-280	-165	133.6	0.08	94.481	8.959
-100	-280	-140	135.2	0.08	131.255	21.935
-100	-250	-195	133.6	0.08	91.706	8.014
-100	-250	-165	134.1	0.08	105.568	10.633
-100	-250	-145	136.2	0.08	135.119	22.069
-100	-220	-195	134.8	0.08	106.201	8.464
-100	-220	-165	134.8	0.08	128.842	17.349
-100	-190	-195	135.1	0.08	138.034	14.124
-100	-190	-180	134.1	0.08	143.432	17.857
-80	-310	-175	135.3	0.08	72.204	8.198
-80	-310	-145	136.9	0.09	87.568	10.823
-80	-310	-125	136	0.08	109.818	12.009
-80	-280	-175	132.9	0.08	75.589	8.297
-80	-280	-145	134.3	0.08	92.327	8.501
-80	-280	-125	136.7	0.08	118.173	16.747
-80	-250	-175	133.1	0.08	80.224	9.955
-80	-250	-145	134.7	0.08	103.09	9.495
-80	-250	-125	136.2	0.08	132.17	20.967
-80	-220	-175	132.8	0.08	93.359	7.229
-80	-220	-145	135	0.08	116.357	14.821
-80	-220	-130	135	0.08	134.821	20.535
-80	-190	-175	134.1	0.08	108.277	9.911
-80	-190	-145	136.3	0.08	139.516	16.92
-80	-160	-175	136.6	0.08	148.35	15.463
-60	-310	-155	137.3	0.08	71.674	8.315
-60	-310	-125	137.2	0.09	83.576	10.642
-60	-280	-155	136	0.08	74.051	8.315
-60	-280	-125	136.6	0.09	88.818	10.156
-60	-250	-155	135.2	0.08	77.278	8.119
-60	-250	-125	138.5	0.09	99.247	9.802
-60	-220	-155	134.4	0.08	82.978	10.181
-60	-220	-125	137.2	0.08	107.591	10.312
-60	-190	-155	135.3	0.08	96.5	8.39
-60	-190	-125	136.5	0.09	121.932	16.762
-60	-160	-155	136.6	0.08	119.891	13.313
-60	-160	-130	137.3	0.08	140.296	19.57
-40	-310	-130	139.6	0.08	70.205	7.951
-40	-280	-130	136.8	0.08	72.667	7.874
-40	-250	-130	136.6	0.08	77.007	7.925
-40	-220	-130	137.3	0.09	81.755	10.014
-40	-190	-130	137.6	0.09	94.281	7.611

Type	S/N	R1	R18	BC	FWHM	Mn tail	RT centroid	RT stdev
		-40	-160	-130	136.9	0.09	106.625	9.902
4231	72030408	-140	-310	-240	142	0.09	81.571	11.191
61kcps		-140	-310	-210	144.6	0.09	101.365	8.524
11% dt		-140	-310	-180	145.3	0.09	131.682	15.997
		-140	-280	-240	142.6	0.09	95.842	8.277
		-140	-280	-210	143.4	0.09	109.118	11.92
		-140	-280	-180	149.2	0.09	152.018	18.799
		-140	-250	-240	143.2	0.09	114.685	11.117
		-140	-250	-210	145.7	0.09	137.421	15.982
		-140	-220	-240	149.8	0.09	154.246	16.049
		-120	-310	-220	144.3	0.09	77.712	8.406
		-120	-310	-190	144.8	0.09	94.317	7.454
		-120	-310	-160	144.5	0.09	120.041	14.416
		-120	-280	-220	143	0.09	88.207	10.009
		-120	-280	-190	142.7	0.09	99.371	9.13
		-120	-280	-165	145.1	0.09	125.527	14.871
		-120	-250	-220	143.5	0.09	99.103	9.261
		-120	-250	-190	143.8	0.09	117.509	13.106
		-120	-250	-170	147.5	0.09	145.397	14.818
		-120	-220	-220	144.7	0.09	123.157	12.722
		-120	-220	-190	147.5	0.09	143.005	16.55
		-100	-310	-195	144.2	0.09	76.637	8.55
		-100	-310	-165	146.1	0.09	93.457	9.493
		-100	-310	-145	144.9	0.09	108.444	12.331
		-100	-280	-195	143.4	0.09	79.269	9.183
		-100	-280	-165	144.5	0.09	96.886	8.989
		-100	-280	-145	146.5	0.09	121.978	15.164
		-100	-250	-195	144.6	0.09	93.377	7.036
		-100	-250	-165	144.2	0.09	107.198	10.182
		-100	-250	-150	144.8	0.09	127.343	13.648
		-100	-220	-195	145	0.09	107.226	9.59
		-100	-220	-165	145.9	0.09	128.792	15.724
		-100	-190	-195	147	0.09	136.6	13.776
		-80	-310	-175	143.7	0.09	72.024	8.123
		-80	-310	-145	145.3	0.09	85.772	11.186
		-80	-310	-130	147.1	0.09	102.022	8.482
		-80	-280	-175	144.8	0.09	77.136	8.208
		-80	-280	-145	144.9	0.09	91.735	7.662
		-80	-280	-130	147.2	0.09	107.233	10.734
		-80	-250	-175	145.5	0.09	84.514	10.661
		-80	-250	-145	145.3	0.09	99.53	9.172
		-80	-220	-175	144.2	0.09	93.956	7.371
		-80	-220	-145	145.4	0.09	113.796	13.345
		-80	-190	-175	145.6	0.09	112.925	12.149

Type	S/N	R1	R18	BC	FWHM	Mn tail	RT centroid	RT stdev
		-80	-190	-145	148.6	0.09	140.969	14.308
		-80	-160	-175	150.5	0.09	149.538	15.446
		-60	-310	-155	147	0.09	74.521	7.868
		-60	-310	-125	146.1	0.09	84.776	11.627
		-60	-280	-155	145	0.09	73.427	8.232
		-60	-280	-125	147.2	0.09	92.958	7.399
		-60	-250	-155	145.8	0.09	79.441	9.434
		-60	-250	-125	147.3	0.09	98.363	9.099
		-60	-220	-155	145.1	0.09	85.903	11.076
		-60	-220	-125	147.1	0.09	106.761	9.624
		-60	-190	-155	147.3	0.09	99.975	8.958
		-60	-190	-125	148.5	0.09	120.981	14.614
		-60	-160	-155	147.2	0.09	116.17	12.737
		-60	-160	-125	152.7	0.09	150.008	19.238
		-40	-310	-130	148.4	0.09	71.45	7.865
		-40	-280	-130	148.3	0.09	74.925	7.35
		-40	-250	-130	148	0.09	78.457	8.266
		-40	-220	-130	147.8	0.09	82.137	10.727
		-40	-190	-130	147.8	0.09	93.595	6.9
		-40	-160	-130	150	0.09	108.809	10.858
Type	S/N	R1	R18	BC	FWHM	Mn tail	RT centroid	RT stdev
8525	72020707	-140	-310	-235	135.5	0.08	82.879	10.834
61 icr		-140	-310	-205	137.9	0.09	102.712	9.399
dt 18 %		-140	-310	-175	135.9	0.08	139.17	18.332
		-140	-280	-235	134.8	0.08	97.712	9.729
		-140	-280	-205	134	0.09	110.939	13.794
		-140	-280	-180	137	0.09	148.451	21.011
		-140	-250	-235	135.2	0.08	117.258	13.804
		-140	-250	-205	136.2	0.1	137.405	20.591
		-120	-310	-210	135.4	0.08	78.028	9.032
		-120	-310	-180	137.1	0.09	97.435	9.819
		-120	-310	-155	135.8	0.08	127.819	15.916
		-120	-280	-210	134.9	0.08	90.367	8.82
		-120	-280	-180	135.5	0.09	104.7	10.041
		-120	-280	-155	136.4	0.08	141.058	16.752
		-120	-250	-210	135.4	0.08	103.935	8.269
		-120	-250	-180	135.6	0.09	124.59	17.444
		-120	-250	-160	138.1	0.09	155.461	24.215
		-120	-220	-210	135.2	0.08	127.69	14.953
		-120	-220	-185	138.1	0.1	147.007	23.301
		-100	-310	-190	137.5	0.09	76.926	8.241
		-100	-310	-160	137.8	0.09	92.598	7.511
		-100	-310	-135	136.1	0.08	119.684	13.458
		-100	-280	-190	135.3	0.08	80.889	10.35
		-100	-280	-160	135.6	0.08	97.586	9.381

Type	S/N	R1	R18	BC	FWHM	Mn tail	RT centroid	RT stdev
		-100	-280	-140	136.6	0.08	121.818	15.54
		-100	-250	-190	135.4	0.08	92.858	7.759
		-100	-250	-160	136.1	0.09	109.688	12.527
		-100	-250	-140	136.7	0.09	139.028	17.881
		-100	-220	-190	135.8	0.08	107.136	10.724
		-100	-220	-160	136.5	0.1	130.272	16.129
		-100	-190	-190	136.3	0.09	138.011	15.311
		-100	-190	-175	138	0.09	148.377	19.756
		-80	-310	-170	138.1	0.08	75.289	7.71
		-80	-310	-140	140.1	0.08	92.544	7.519
		-80	-280	-170	136	0.08	77.066	8.705
		-80	-280	-140	137.3	0.08	94.138	7.097
		-80	-250	-170	136.8	0.08	83.08	10.331
		-80	-250	-140	138.3	0.09	103.857	8.952
		-80	-220	-170	136	0.08	94.589	7.239
		-80	-220	-140	137.5	0.09	113.575	13.623
		-80	-190	-170	137.1	0.09	113.156	12.644
		-80	-190	-140	139.4	0.1	143.361	18.171
		-80	-160	-170	138.8	0.09	151.275	19.54
		-60	-310	-145	140.2	0.08	74.943	7.526
		-60	-310	-125	138.1	0.09	79.492	9.154
		-60	-280	-145	137	0.08	75.135	7.888
		-60	-280	-125	140.2	0.09	89.023	9.509
		-60	-250	-145	136.8	0.09	79.279	9.308
		-60	-250	-125	140.3	0.09	94.898	7.315
		-60	-220	-145	138.3	0.08	91.471	7.564
		-60	-220	-125	139	0.09	102.019	8.175
		-60	-190	-145	137.4	0.08	102.227	7.601
		-60	-190	-125	138.3	0.09	119.687	12.918
		-60	-160	-145	137.7	0.09	125.69	13.538
		-60	-160	-125	139.6	0.1	143.149	16.485
		-40	-310	-125	139.7	0.09	70.752	8.146
		-40	-280	-125	139.4	0.09	74.398	8.072
		-40	-250	-125	138.9	0.09	77.474	8.033
		-40	-220	-125	138.1	0.09	82.034	9.972
		-40	-190	-125	139.6	0.09	94.707	7.47
		-40	-160	-125	138.7	0.09	107.354	10.296
Type	S/N	R1	R18	BC	FWHM	Mn tail	RT centroid	RT stdev
4231	72030308	-140	-310	-240	141.4	0.09	86.114	11.199
icr 62k		-140	-310	-210	142.8	0.09	105.012	9.5
dt 11%		-140	-310	-185	143.5	0.1	125.512	16.727
		-140	-280	-240	141.8	0.09	100.672	9.445
		-140	-280	-210	143.8	0.09	120.838	15.334
		-140	-250	-240	142.5	0.09	123.417	13.608
		-140	-250	-225	145.5	0.1	133.188	18.034

-120	-310	-220	142.4	0.09	82.327	10.42
-120	-310	-190	143.1	0.09	97.014	9.003
-120	-310	-165	143.1	0.1	117.222	14.393
-120	-280	-220	141.8	0.09	92.299	7.215
-120	-280	-190	143.2	0.09	107.601	9.886
-120	-280	-170	146	0.1	129.777	16.525
-120	-250	-220	142.8	0.09	105.685	8.311
-120	-250	-190	144.2	0.09	124.248	17.846
-120	-220	-220	145.2	0.1	133.179	13.756
-100	-310	-200	143.5	0.1	77.739	8.357
-100	-310	-170	145.2	0.09	96.301	8.168
-100	-310	-145	144.7	0.1	115.506	12.744
-100	-280	-200	142.6	0.1	83.714	10.548
-100	-280	-170	142.7	0.09	98.124	9.3
-100	-280	-145	144.5	0.1	127.818	15.449
-100	-250	-200	143.4	0.09	94.254	7.478
-100	-250	-170	144.8	0.09	112.743	13.689
-100	-250	-150	147.6	0.1	137.256	15.972
-100	-220	-200	143.3	0.1	109.408	11.326
-100	-220	-170	145.9	0.1	130.493	14.717
-100	-190	-200	147.9	0.1	141.496	15.738
-80	-310	-180	145.8	0.1	76.257	7.522
-80	-310	-150	144.5	0.09	89.017	9.986
-80	-310	-130	145.5	0.1	106.649	7.544
-80	-280	-180	144.4	0.1	78.721	8.242
-80	-280	-150	144	0.1	93.92	7.641
-80	-280	-130	145	0.1	112.606	11.074
-80	-250	-180	143.8	0.09	86.847	11.051
-80	-250	-150	145.3	0.1	104.143	8.321
-80	-250	-130	145.3	0.1	126.327	14.009
-80	-220	-180	144	0.09	96.799	7.642
-80	-220	-150	145.8	0.1	118.212	14.245
-80	-220	-135	148.7	0.1	140.569	17.04
-80	-190	-180	146.7	0.1	120.771	12.987
-80	-190	-155	149.1	0.1	138.617	14.799
-60	-310	-155	146.1	0.1	75.88	7.513
-60	-310	-125	147.3	0.1	93.064	7.641
-60	-280	-155	145.5	0.1	77.38	7.82
-60	-280	-125	145.4	0.1	94.446	6.971
-60	-250	-155	144.3	0.09	80.07	9.16
-60	-250	-125	145.9	0.1	102.94	7.771
-60	-220	-155	145.9	0.1	90.675	8.566
-60	-220	-125	147.3	0.1	117.765	12.369
-60	-190	-155	146.4	0.1	106.929	8.755
-60	-190	-125	148.1	0.1	133.223	13.017

Type	S/N	R1	R18	BC	FWHM	Mn tail	RT centroid	RT stdev
		-60	-160	-155	148	0.1	130.369	13.226
		-60	-160	-140	150.2	0.1	138.168	13.377
		-40	-310	-130	147.7	0.1	76.044	7.484
		-40	-280	-130	146.6	0.1	76.713	7.978
		-40	-250	-130	147.3	0.1	82.694	10.082
		-40	-220	-130	147.6	0.1	89.102	9.451
		-40	-190	-130	148.6	0.1	100.766	8.566
		-40	-160	-130	149.4	0.1	120.048	12.602
8525	72060307	-140	-310	-235	136.1	0.06	82.719	10.394
icr 64k		-140	-310	-205	135.8	0.06	102.803	7.06
dt 18%		-140	-310	-175	137.8	0.07	143.579	12.368
PASS		-140	-280	-235	136.2	0.07	103.197	6.631
FWHM	135.04	-140	-280	-205	136.8	0.07	121.146	11.518
Mn tail	0.06	-140	-280	-180	138.8	0.07	157.725	16.045
R1	-120	-140	-250	-235	137.3	0.06	122.375	12.203
R18	-250	-140	-250	-205	138.3	0.07	149.129	16.469
BC	-215	-140	-220	-235	139.7	0.07	173.111	16.029
		-120	-310	-210	136.8	0.07	79.478	9.723
		-120	-310	-180	136.6	0.07	98.828	9.145
		-120	-310	-160	136.7	0.07	122.719	11.316
		-120	-280	-210	135.9	0.06	92.191	6.711
		-120	-280	-180	137.3	0.07	110.049	10.313
		-120	-280	-160	138	0.07	143.127	11.6
		-120	-250	-210	136.7	0.07	107.725	9.133
		-120	-250	-180	137.4	0.07	130.686	11.783
		-120	-250	-165	137.9	0.07	154.441	15.82
		-120	-220	-210	137.7	0.07	134.726	11.172
		-120	-220	-180	139.4	0.07	166.284	19.853
		-100	-310	-190	137.2	0.06	76.676	8.134
		-100	-310	-160	140.1	0.06	99.816	8.479
		-100	-310	-140	138.2	0.07	119.893	11.817
		-100	-280	-190	137.4	0.07	84.439	10.887
		-100	-280	-160	136.4	0.06	102.193	7.162
		-100	-280	-145	138.3	0.07	122.8	11.353
		-100	-250	-190	137.8	0.06	95.794	8.082
		-100	-250	-160	137.5	0.07	116.846	11.698
		-100	-220	-190	136.9	0.06	110.724	10.102
		-100	-220	-160	138.1	0.07	141.145	12.424
		-100	-190	-190	138.8	0.07	144.614	13.712
		-100	-190	-170	140.3	0.07	168.036	17.421
		-80	-310	-170	139.9	0.07	76.379	7.594
		-80	-310	-140	139.5	0.07	93.592	6.462
		-80	-280	-170	137.6	0.06	79.804	9.034
		-80	-280	-140	139.9	0.07	100.741	7.751

Type	S/N	R1	R18	BC	FWHM	Mn tail	RT centroid	RT stdev
		-80	-250	-170	136.9	0.06	85.205	10.749
		-80	-250	-140	139.1	0.07	107.628	9.461
		-80	-220	-170	137.8	0.06	100.81	7.796
		-80	-220	-140	138.5	0.07	122.163	10.673
		-80	-190	-170	138.3	0.07	116.457	11.711
		-80	-190	-140	140.2	0.07	151.575	14.568
		-80	-160	-170	141	0.07	164.839	14.039
		-60	-310	-145	140.7	0.07	75.988	7.553
		-60	-310	-125	140.5	0.07	86.07	11.057
		-60	-280	-145	137.9	0.07	77.991	8.052
		-60	-280	-125	140.2	0.07	92.908	7.073
		-60	-250	-145	138.1	0.06	84.594	10.505
		-60	-250	-125	139.4	0.07	98.462	8.65
		-60	-220	-145	138.2	0.07	92.784	6.855
		-60	-220	-125	140.6	0.07	111.055	9.635
		-60	-190	-145	138.3	0.07	106.661	7.85
		-60	-190	-125	139.9	0.07	124.192	11.377
		-60	-160	-145	139.6	0.07	134.251	10.038
		-60	-160	-125	140.9	0.07	159.586	13.465
		-40	-310	-125	142.5	0.07	75.205	7.889
		-40	-280	-125	140.5	0.07	77.099	8.153
		-40	-250	-125	139.8	0.07	79.19	8.609
		-40	-220	-125	139.9	0.07	86.638	10.67
		-40	-190	-125	140.9	0.06	98.734	8.702
		-40	-160	-125	140.4	0.07	115.217	10.689
Type	S/N	R1	R18	BC	FWHM	Mn tail	RT centroid	RT stdev
8525	72060408	-140	-310	-235	140	0.09	89.356	9.54
icr 54k		-140	-310	-205	140	0.08	105.357	9.78
dt 16%		-140	-310	-180	139.4	0.08	134.213	14.168
		-140	-280	-235	137.9	0.08	100.967	8.657
		-140	-280	-205	137.7	0.08	117.982	12.978
		-140	-280	-185	139.6	0.08	145.515	13.663
		-140	-250	-235	138.1	0.08	121.403	12.319
		-140	-250	-205	139.3	0.08	146.884	14.47
		-140	-220	-235	141.8	0.08	172.31	18.516
		-120	-310	-215	138.6	0.08	78.311	8.641
		-120	-310	-185	140.6	0.09	99.317	9.421
		-120	-310	-160	139.4	0.08	125.683	13.394
		-120	-280	-215	138.4	0.08	91.666	7.647
		-120	-280	-185	138.1	0.08	105.918	9.204
		-120	-280	-165	139.3	0.08	131.258	13.549
		-120	-250	-215	139	0.08	104.648	8.01
		-120	-250	-185	137.9	0.08	124.328	13.637
		-120	-250	-165	141.1	0.08	157.446	18.141
		-120	-220	-215	139.2	0.08	130.346	11.818

-120	-220	-185	140.4	0.08	157.719	17.537
-120	-190	-215	146.3	0.09	191.894	21.152
-100	-310	-195	140.6	0.08	76.942	8.005
-100	-310	-165	140.5	0.09	94.742	7.624
-100	-310	-145	139.3	0.09	113.228	10.6
-100	-280	-195	139.3	0.08	82.407	10.537
-100	-280	-165	138	0.08	100.177	8.767
-100	-280	-145	140	0.08	126.065	13.855
-100	-250	-195	138.2	0.08	94.878	6.853
-100	-250	-165	139.1	0.08	112.086	11.066
-100	-250	-150	140.2	0.09	132.092	12.609
-100	-220	-195	138.7	0.08	109.26	10.166
-100	-220	-165	139.7	0.08	134.767	11.324
-100	-190	-195	139.2	0.08	142.557	13.767
-100	-190	-170	142.3	0.09	165.029	18.5
-80	-310	-170	140.8	0.08	76.665	8.112
-80	-310	-140	141.1	0.09	93.591	7.94
-80	-280	-170	138.7	0.08	80.224	9.28
-80	-280	-140	139.6	0.08	98.885	9.16
-80	-250	-170	138.9	0.08	88.208	10.071
-80	-250	-140	141.8	0.08	111.203	11.227
-80	-220	-170	139.7	0.08	101.77	7.886
-80	-220	-140	140.6	0.08	126.445	13.036
-80	-190	-170	139.5	0.08	122.15	11.656
-80	-190	-140	142.2	0.08	153.853	16.719
-80	-160	-170	142.8	0.08	164.361	18.829
-60	-310	-150	141.2	0.08	74.46	7.46
-60	-310	-125	142.1	0.09	88.444	10.243
-60	-280	-150	140.3	0.08	77.781	8.055
-60	-280	-125	143	0.08	95.357	8.06
-60	-250	-150	140.6	0.08	81.985	10.107
-60	-250	-125	141.8	0.08	102.788	8.13
-60	-220	-150	139.5	0.08	92.699	6.891
-60	-220	-125	141.6	0.08	112.423	11.477
-60	-190	-150	140.2	0.08	104.984	7.815
-60	-190	-125	141.1	0.08	129.043	15.1
-60	-160	-150	141.2	0.08	132.285	11.994
-60	-160	-130	142.4	0.08	150.791	14.032
-40	-310	-125	145.3	0.08	77.064	7.283
-40	-280	-125	142.6	0.08	77.847	7.617
-40	-250	-125	142.3	0.08	82.356	10.065
-40	-220	-125	141.7	0.08	92.091	7.29
-40	-190	-125	141.5	0.08	100.851	8.666
-40	-160	-125	142.8	0.09	119.149	12.799